# 13.56 MHz antenna design for dynamic EV charging system

A DISSERTATION SUBMITTED TO THE
GRADUATE SCHOOL OF ENGINEERING AND SCIENCE OF
SHIBAURA INSTITUTE OF TECHNOLOGY

by

**NGUYEN TRI CUONG**

IN PARTIAL FULFILLMENT OF THE REQUIREMENTS
FOR THE DEGREE OF

**DOCTOR OF PHILOSOPHY**

MAY 2020

# Acknowledgments

First of all, I would like to convey my special thanks to my supervisor, Professor Akatsu Kan for his kindness, encouragements, enthusiastic guidance, helpful advices and technical supports throughout my research.
I would also like to thank to all students in ME Energy Conversion laboratory, Shibaura Institute of Technology and special thanks to my all Vietnamese friends for their support.

Saitama, May, 2020

Nguyen Tri Cuong

# Abstract

In the present, energy and environment are concerned. In daily life and production, transport is very important. It also consumes a lot of energy. Gasoline and oil are used in common. They have the high energy density but they are limited. Moreover, the emissions are the major issues when fossil energy is used. Hence, the electrification for transportation has been carrying out for many years. A train can get electric power easily because it runs on a fixed rail. It's not easy for the electric vehicle (EV) to get power in a similar way. Therefore, the EV has to equip a large and heavy battery pack. It is very necessary for a long trip. And people have to connect the vehicle to power source for a long time to charge the battery. It is not convenient. Dynamic charging by using wireless power transfer (WPT) is a solution. It can increase the moving distance and reduce the battery capacity. In this dissertation, the design of the 13.56 MHz antenna and the efficiency improvement of the dynamic charging system are presented.

Firstly, the strongly coupled magnetic resonance is analyzed in coupled mode theory and circuit theory.

Secondary, the 13.56 MHz antenna is analyzed and designed by finite element analysis. The simulation result of the over 90% antenna at 50 cm is shown. The physical model of the antenna is created. It can operate in the wireless power transfer system.

Lastly, the problem of the wireless dynamic charging system is presented. Moreover, the proposed solution to improve the efficiency of the antenna the system is shown. The efficiency of the antenna can be inceased in the charging area. The results are shown in simulation and experiments.

# Contents

# List of Figures

# List of Tables

# List of Algorithms

$f_r$ : Resonant Frequency
$L$ : Self-Inductance
$C_p$ : Parasitic Capacitance
$\omega$ : Angular Frequency
$a_\pm$ : Mode Amplitude
$C$ : Capacitance
$W$ : Energy Stored inside Circuit
$\Gamma$ : Decay Rate of the Circuit
$P_{loss}$ : Dissipated Power inside the Circuit
$Q$ : Quality Factor of Circuit
$\Gamma_{ext}$ : Decay Rate of Power Loss in a Waveguide
$Q_{ext}$ : External Quality Factor
$K$ : Coupling Coefficient
$s_+$ : Incident Wave
$|s_-^2|$ : Input Power
$k_{12,21}$ : Coupling Coefficient between Resonator 1& 2
$P_{21}$ : Power Transferred from First Resonator to Secondary Resonator
$I_{1,2}(t)$ : Current Envelope Quantity
$\dot{\bar{a}}$ : Vector of the Mode Amplitude
$V_{1,2}$ : Eigen Vector
$\eta$ : Transfer Efficiency
$S_{21}$ : Transmission Coefficient
$S_{11}$ : Reflection Coefficient
$Z_{11,22,12,21}$ : Impedance Matrix

## LIST OF ALGORITHMS

$Z_s$ : Source Impedance
$Z_{in}$ : Input Impedance
$Z_L$ : Load Impedance
$Z_{out}$ : Output Impedance
$\eta_1$ : Transfer Efficiency
$Z_2$ : Reflected Impedance from Secondary Circuit to Primary
$R_L$ : Load Resistance
$a$ : Helical Coil Radius
$N$ : Number of Turns
$h$ : Height of Helical Coil
$L_s$ : Self-Inductance of Helical Coil
$k_f$ : Non-Uniformity Coefficient
$k_s$ : Conductor Shape Coefficient
$k_m$ : Mutual Inductance Coefficient
$C_{tt}$ : Turn-to-Turn Capacitance
$C_{ts}$ : Turn-to-Shield Capacitance
$R_p$ : Total Internal Resistance

# Chapter 1

# Introduction

## 1.1 Wireless power transfer

In the basic law of thermodynamics; the law of conservation of energy, energy may neither be created nor destroyed just can be transformed. Nature is the best example of this physics fundamental law, in fact they are the expert at conserving it. Life and evolution of species are all favoured to this law and become so accustomed to living under it that we did not pay attention to its existence and how it influence our life.

When man first discovered the use of fire, the first thing he tried was to transfer it back to its shelter. Since back then, we have been manupulating the use of nature's energy for our own purpose and benefit. Later, man began to discover fuels and gather mineral charcoals, vegetable charcoal and among others which then be be transformed into heat and light. From then on the development of energy transportation become more and more important resulting to the invention of electrical energy. Through that, the biggest energy network human kind has ever built was invented, the electrical grid. Such grid, open doors to broader limit where science are now more oriented on optimizing the efficiency on driving such energy. However, even if high efficiency is able to be achieved, it is inenvitable to lose some of the energy through unwanted reasons.

For decades, electrical energy is being transferred using cables and wires. But this limits electrical energy to places that are harder to reach such as inside the human body, or isolated spaces. To overcome the problem, energy transportation without the use of cable is introduced. Some of the potential application that can implement the technology includes:

- Medical Field. The development in medical field allow doctors to perform treatment using electrical devices implants, such as pacemakers, cochlers implants etc.
- Power Charging. Electrical device, electric vehicle and unmanned aircraft.
- Home appliance such as vaccuum cleaners, irons and televisions.

Above mentioned potential application sparks interest in wireless energy transfer. Such techlonogy is not impposible, because nature has been doing energy distribution a long time ago without the use of cables. For example, solar power. Nature retrives the energy from sunlight to drive the photosysnthesis process and generates nutrients that later is being used to motor the food chain and life. At present, several solar power technology has been developed to harvest the energy from sunlight and transformed it into electrical power. Among them was photovoltaic cells. After this energy is collected, the next step needed to be considered is distributing the power. This is where cables and wires becomes importamt. However as being noted before, physical transfer has limits. Moreover, they also play an important part in contributing to the unwanted energy loss. In early 1889, Nikola Tesla performed the first wireless power transfer by inventing the famous Tesla coils. Since then, wireless power transfer gain the attention from researchers from around the world.

In the early 19th century when Tesla first performed his first experiments, he achieved an incredible result, where it has been said that he managed to light up bulbs several kilometers away. However, due to the dangerous nature of the experiment in exchange for low efficiency power transfer, the experimentation was abandoned. Tesla left his legacy with patent that was never been exploited commercially.

For wireless transmission of information, electromagnetic radiation is often being used. These information travels in form of energy on the electromagnetic waves. Theoretically, it is possible to transfer energy similarly to this method that has been used to transfer data. In 1964, William C. Brown proposed a point to point wireless power transfer scheme on the basic of microwave beam [3].

Glaser (1973) showed that it is possible to transfer energy directionally using microwaves. Although this method is very efficient, it has few disadvantages that are unavoidable. For one, the method requires a direct line of sight to transfer energy. Which means it can cause great harm to living mechanism that accidentally crosses the path. To overcome this, another option is introduced, electromagnetic resonance. Even though electromagnetic resonance has a short distance limit, it can achieve high efficiency wireless power transfer. According

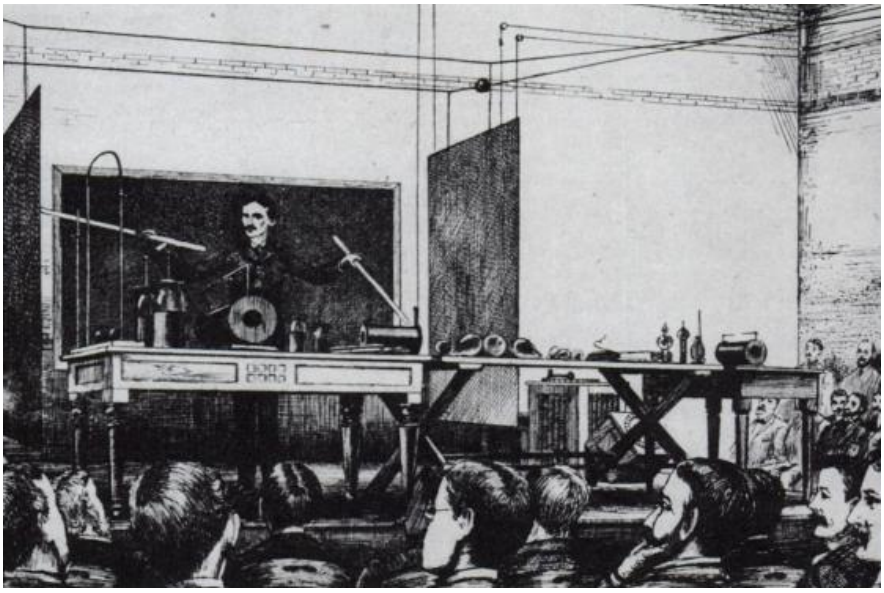

Figure 1.1: Nikola Tesla demonstrates the wireless power transfer at Columbia Collegeretrieved

to Karalis et al.(2008) [15], Kurs(2007) [17], the resonant coupling does not effect to human health.

Presently, there are diverse type of physical mechanisms for wireless power transfer, such as:

- Laser. This method falls under the far-field or radiating techniques. This techniques achieves high efficiency for larger distance, often involves multiple kilometers range. Longer range in this method is possible due to the electromagnetic radiation or beam is made to match the intended area of the receiver. In this method, electrical power is transformed in laser beam and is pointed at photovoltaic cells. The receiver is then convert the beam back into electrical energy. In 2003, NASA invented a remote-controlled aircraft that are wirelessly energized by laser beam by placing photovoltaic cell as the energy collector.

- Radio waves and Microwaves. This method also falls under the far-field wireless power transfer. Power transmission using radio wave allows longer

distance power beaming using shorter length of electromagnetic radiation in microwave range. Glaser (1973) shown how high power energy can be transmitted using microwaves.

- Inductive Coupling. This method is classified under the near-field techniques where the magnetic field dissipates quickly when the transfer range is about one diameter of the antenna. Inductive coupling is based on the theory of magnetic field created by the electric current to induce a secondary current on the secondary conductor. The disadvantage of this technique is the short limit range between the primary source and the secondary conductor.

- Strongly Coupled Magnetic Resonance. Karalis et al.(2008) [15], Kurs(2007) [17] introduced the method of strongly coupled magnetic resonance wireless power transfer.

The mechanical resonance or acoustic is known is physic which consists in applying a vibratory periodic action with a vibratory period that match the maximum absorption energy rate of an object. That frequency of period is called resonant frequency. The effect of this resonant frequency can be destructive. For example, rigid object such as bridge or building can collapse when the resonance frequency is achieved accidentally caused by the wind or earthquake. Resonance does not only exist in mechanisms, it is also exist in electricity. This resonance is known electrical resonance or inductive resonance. Using this phenomenon, we can transfer energy wirelessly and maximum energy absorption is possible when the intended object is in resonance with each other. When two objects with the same resonant frequency is coupled together, one object can transfer its energy to the other efficiently.

Inductive coupling is a mechanism where the resonant coupling takes place between coils of two LC circuits with the same resonant coupling [21, 22, 23, 26, 39, 40]. In Fig. 1.2(a), the energy from the transmitting coil is transferred to the receiving coil when both coil is resonant at the same frequency.

According to [15], self resonance occur naturally in all coils(L). The resonant frequency of the coil can be expressed by

$$f_r = \frac{1}{\sqrt{LC_p}} \tag{1.1}$$

where $C_p$ is the parasitic capacitance of the coil. And Karalis showed that it is possible to achieve good efficiency with the coupling scheme shown in Fig. 1.2(b). To achieve the efficiency of 40%, the radius (a) of the coil must be much lower than the wavelength ($\lambda$) of the resonant frequency. And the maximum range between the two coils must satisfies the condition of $a \leq d \leq \lambda$, to achieve the optimum coupling.

Even though, Inductive coupling is similar to this method, the two fundamental differences that separates this method from inductive coupling is that the capacitance of the LC circuit is parasitic, not discrete. The self-resonant frequency of the coils depends on the parasitic capacitance, and since this value is very small, the self-resonant frequency of coil tends to be very high (around GHz). To reduce this resonant frequency, thick copper wire and largely spaced wire is necessary to bring the frequency down to megahertz range.

## 1.2 EV dynamic charging system

Recently, Electric Vehicles (EVs) are a solution for reducing CO2 emission and air pollution in the world. However, the EVs have been not attractive to the consumers due to the short running distance, long charging time and high battery cost. Hence, the Dynamic Wireless Charging (DWC) solution has been proposed to reduce the energy dependence and battery cost of EVs [2, 5, 6, 7, 12, 14, 18, 20, 35, 37].

The WPT technology had been researching to apply in EVs charging from several years ago. In the late of 1970s, a 20kW WPT system was conducted for a running EV [2]. The wireless transfer distance was 2.5 cm. Huge couplers were used because of the using only 180 Hz frequency. By the development of power electronic, the frequency has been increasing to reduce the antenna size while

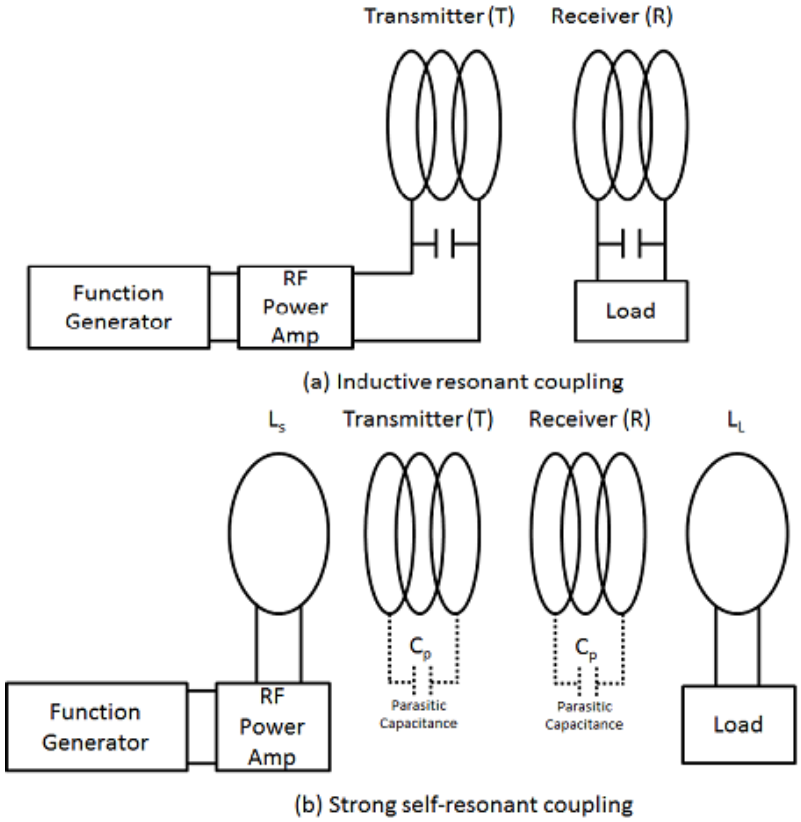


Figure 1.2: Coupling Scheme. (a) Inductive Resonant Coupling and (b) is Strong Self-Resonant Coupling

increase the transfer distance and obtain high efficiency. In the recent technology, as shown in Fig. 1.3, the EV WPT systems are almost using frequency in range from 20 kHz to 150 kHz [5, 18, 24, 27, 29, 35, 38, 42].

A few hundred millimetres transfer distance with over 90% efficiency was achieved at kilowatt power level. In MHz frequency range, the size and weight of the coupling coils are much reduced. The transfer distance can expand to more than 1 meter with transfer efficiency over 90% [17]. These features promise a great performance for EV dynamic charging systems. In this project, we will build a WPT system for EV DWC applications with the transfer distance is up to 1 meter. Therefore, the 13.56 MHz frequency in ISM band is chosen. However, in MHz operation frequency is still hard to apply in EV charging system because

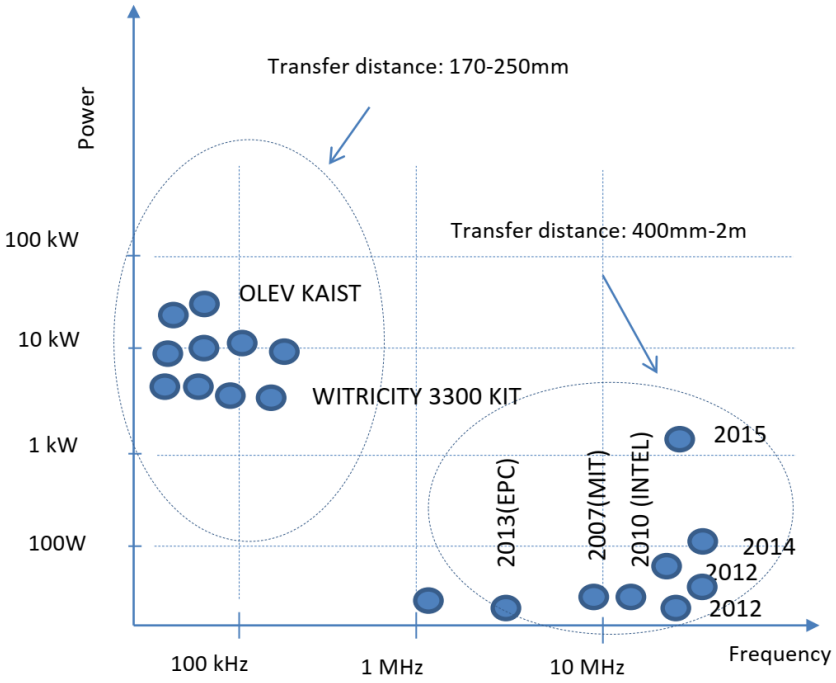


Figure 1.3: Transfer power versus operating frequency

it's difficult to transfer several kilowatts power with high efficiency [18].

The structure of a dynamic EV charging system is shown in Fig. 1.4. It includes the transmitting side in the charging station and the receiving side in the vehicle. In the transmitting side, the electrical energy is converted to the 13.56 MHz frequency power source by a rectifier and a high frequency inverter. The receiving side receives the power by the 13.56 MHz antenna. Then, the power is charged to the battery by a high frequency rectifier and an impedance matching and charging control. With the current technology, the efficiency of dynamic EV charging system depends on the efficiency of the 13.56 MHz antenna. Base on the standards about power levels and efficiency of EV WPT which is recommended in the developing SAE J2954 standard [11], the efficiency of over 85% for whole system is recommended. To satisfy such efficiency, the efficiency of each part in the dynamic EV charging system is shown in Fig. 1.4. The efficiency of over 92% for 13.56 MHz high power antenna is required.

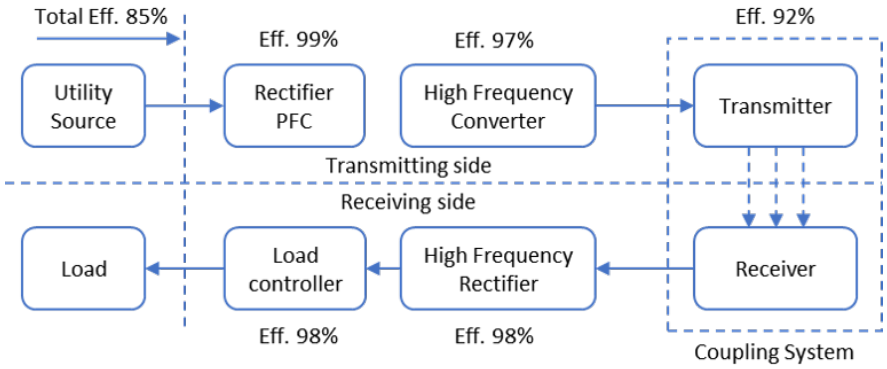


Figure 1.4: Structure of WPT system

## 1.3 Research challenges

Base on the requirement of the antenna, three major research challenges are recognized in this project as following:

• Firstly, the analysis of the antenna theory is presented. The couple mode theory and the scattering matrix's parameters method will be shown. Theo theory shows the effect of the antenna's parameters to the transfer power and efficiency. It also presents the solution to achieve the high efficiency at operating frequency.

• Secondly, the 13.56 MHz high efficiency antenna is designed by Finite Element (FE) simulation. The over 90% efficiency and 50 cm transfer power antenna are the optimal design. These results are compared to the experimental results. However, the difference between the results are presented. Moreover, the design is only compatible to the static WPT system because of the narrow band width of the high efficiency.

• Thirdly, the efficiency of the antenna is improved in the charging area with the supporting system. The system can compensate the variation of the receiving side's position. As the result, the efficiency of the antenna is increased maximum 56% than the previous system within 55 cm transfer system and 40 cm misalignment.

## 1.4 Dissertation outline

This dissertation includes of four chapters. Chapter 1 introduces about the summarisation of WPT, the EV dynamic charging system, the requirements, challenges of the research which is presented in this dissertation. The analysis of the antenna is presented in chapter 2. Chapter 3 presents the design of high efficiency at 13.56 MHz operating frequency antenna. The equation and the simulation method are also descripted in this chapter. The transfer distance 50 cm and 500W power transfer are also obtained. Finally, the improvement of efficiency due to charging area of DWC system is presented in chapter 4.

# Chapter 2

# The Analysis Of The Antenna

## 2.1 Introduction

In this chapter the analytical model of a wireless power transfer scheme is developed through the means of Coupled Mode Theory (CMT). The derivation is made under the assumption of low internal coil losses and some particular type of resonator (coil inductance and capacitance) equivalent circuit. With the equivalent circuit modeling the wireless power transfer system the direct high frequency power source connection to the source coil. At MHz frequencies especially near and at the resonant frequencies, the calculation of coil parameters which are the coefficients of the model obtained by means of CMT is not a trivial task. Equivalent resistance, capacitance and inductance of antenna become frequency dependent, and those should be specially considered. Because the equivalent resistance is a critical parameter for the efficiency maximization, the skin and proximity effects are included and the verification of the calculation process is presented. Also due to frequency dependence of equivalent inductance and capacitance, the procedure to obtain the optimal resonant frequency of antennas in terms of the efficiency of the power transfer is discussed.

## 2.2 Analysis based on the Coupled Mode Theory

Resonance phenomenon can take many forms such as mechanical resonance, acoustic resonance, electromagnetic resonance electron spin resonance etc. The wireless power transfer is based on electromagnetic resonance and can be discussed by the means on CMT.

### 2.2.1 Simple Lossless LC Circuit

Fig 2.1 shows the ideal lossless LC circuit. From this circuit, we can derive the following equation.

$$v = L\frac{di}{dt}; \quad i = -C\frac{dv}{dt} \tag{2.1}$$

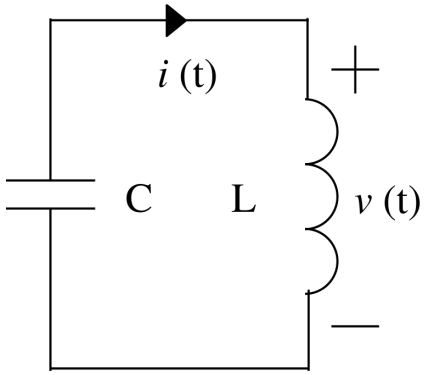


Figure 2.1: Simple Lossless LC Circuit

expressing this equation in one second order differential equation, we get,

$$\frac{d^2v}{dt^2} + \omega^2 v = 0 \tag{2.2}$$

Where $\omega = 1/\sqrt{LC}$ is the resonant frequency of the $LC$ circuit. Also, instead of a set of two coupled differential equation in (2.1), two undoupled differential equations can be derived as (2.4) and(2.5) by defining the new complex variables defined in (2.3).

$$a_{\pm} = \sqrt{\frac{C}{2}}(v \pm j\sqrt{\frac{L}{C}}i) \tag{2.3}$$

By using $a_+$ and $a_-$ (mode amplitude) it is possible to derive the system equations as (2.4) and (2.5).

$$\frac{da_+}{dt} = j\omega a_+ \tag{2.4}$$

$$\frac{da_-}{dt} = j\omega a_- \tag{2.5}$$

The square mode amplitude is the energy stored in the circuit. We can verify this by considering the following equation,

$$v(t) = |V|\cos(\omega_0 t) \tag{2.6}$$

$$i(t) = \sqrt{\frac{C}{L}}|V|\sin(\omega_0 t) \tag{2.7}$$

where, the $|V|$ is voltage peak amplitude. To derive the mode amplitude $a$, we can substitute (2.6) and (2.7) into (2.3).

$$a_+ = \sqrt{\frac{C}{L}}(|V|\cos(\omega_0 t) + j|V|\sin(\omega_0 t)) = \sqrt{\frac{C}{2}}|V|e^{j\omega_0 t} \tag{2.8}$$

Hence,

$$|a_+|^2 = \frac{C}{2}V^2 = W \tag{2.9}$$

where $W$ is the energy stored in the circuit.

### 2.2.2 LC Circuit with Loss

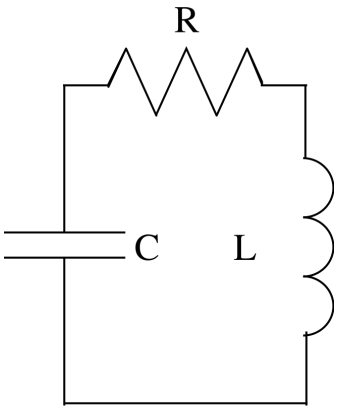


Figure 2.2: Lossy LC Circuit

Usually in real circuit, loss is exits. Fig 2.2 shows the equivalent LC circuit with loss. Using the pertubrbation theory assumpation, equation (2.4) can be expressed into (2.10)

$$\frac{da}{dt} = j\omega a - \Gamma a \tag{2.10}$$

where $\Gamma$ is the decay rate of the circuit. In this case, the decay rate can be calculated from (2.5), and from calculating the relation of power and mode amplitude $a$. From (2.9), the decay rate can be expressed by,

$$\frac{d|a|^2}{dt} = \frac{dW}{dt} = -2\Gamma W = -P_{loss} \tag{2.11}$$

where $P_{loss}$ is a power dissipated on the resistance, and (2.11) can be transformed to

$$P_{loss} = \frac{1}{2}|I|^2 R = \frac{WR}{L} \tag{2.12}$$

In case the circuit is not loaded, the quality factor $Q$ of the system is expressed as follow.

$$Q = \omega \frac{W}{P_{loss}} = \frac{\omega}{2\Gamma} = \frac{\omega L}{R} \tag{2.13}$$

From here, the decay rate can be derived as (2.14)

$$\Gamma = \frac{R}{2L} \tag{2.14}$$

When other pertrubations is needed (coupling with other resonator, transmission line connection, etc.), it will be added in a similar way to the intrinsic circuit loss.

### 2.2.3 Lossy Circuit with Power Source

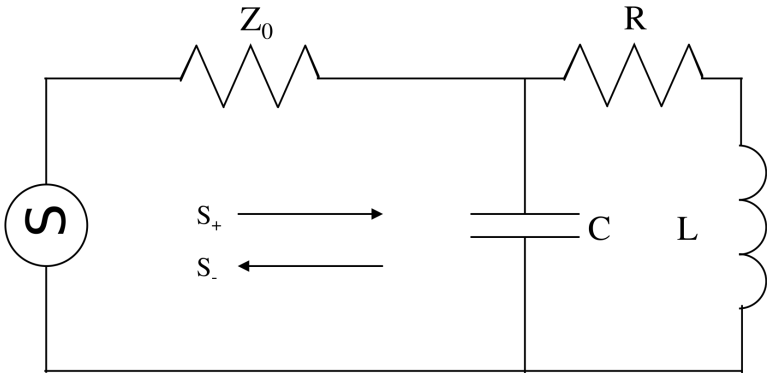


Figure 2.3: Resonant circuit with external source and waveguide

When power source is introduced to system as Fig 2.3, the following modification is required.

- Decay rate modification
- Mode amplitude excitation due to incident wave.

Decay rate is modified due to loss not only from the coil but also from the 'waveguide' connecting source to antenna. Hence, equation (2.10) should be modified to

$$\frac{da}{dt} = j\omega a - (\Gamma_{ext} + \Gamma)a \tag{2.15}$$

where $\Gamma_{ext}$ is the decay rate of the power loss in a waveguide. The product of the external decay rate and energy stored in the system should be linearly proportional to the power dissipated in awaveguide, so $\Gamma_{ext}$ can be calculated from,

$$Q_{ext} = \frac{\omega}{2\Gamma_{ext}} \tag{2.16}$$

where $Q_{ext}$ is the external quality factor. When considering incident wave, (2.15) becomes (2.17).

$$\frac{da}{dt} = j\omega a - (\Gamma_{ext} + \Gamma)a + Ks_+ \tag{2.17}$$

where $K$ is the coupling coefficient between the source and the resonators. $s_+$ is the incident wave incoming to the antenna and $|s_+^2|$ is the input power. Using the Maxwell's euqations,

$$K = \sqrt{2\Gamma_{ext}} \tag{2.18}$$

and from here, the resonators mode can be describe as follow.

$$\frac{da}{dt} = j\omega a - (\Gamma_{ext} + \Gamma)a + \sqrt{2\Gamma_{ext}}s_+ \tag{2.19}$$

### 2.2.4 Coupling between Two Lossless Resonant Circuits

From the formalism presented berforehand, it is possible to describe the coupling between two resonant circuit as shown in Fig 2.4. Suppose that $a_+$ and $a_-$ is the mode amplitude of two uncoupled lossless resonators. Both of the resonators has different resonant frequency of $\omega_1$ and $\omega_2$ respectively. When the two resonators is coupled under some perturbation condition (in wireless power transfer case it is Mutual Inductance,$M$), the frist resonators can be expressed as (2.20).

$$\frac{da_1}{dt} = j\omega a_1 + k_{12}a_2 \tag{2.20}$$

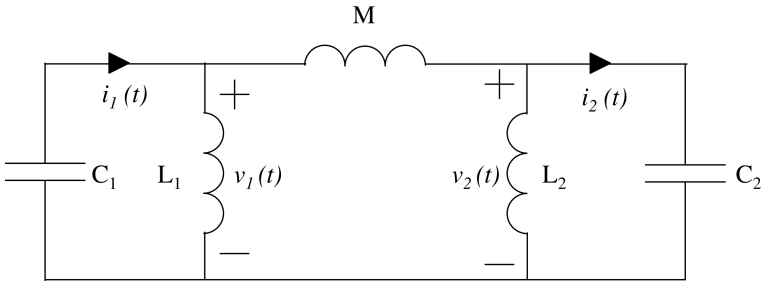


Figure 2.4: Coupled Resonators

and the second resonators is expressed as

$$\frac{da_2}{dt} = j\omega a_2 + k_{21}a_1 \tag{2.21}$$

where $k_{12}$ and $k_{21}$ is the coupling coefficient between the resonators. The condition between the two resonators is defined using the energy conservation law in (2.22).

$$\frac{d}{dt}(|a_1|^2+|a_2|^2) = a_1\frac{da_1^*}{dt}+a_1^*\frac{da_1}{dt}+a_2\frac{da_2^*}{dt}+a_2^*\frac{da_2}{dt} = a_1^*k_{12}a_2+a_1k_{12}^*a_2^*+a_2^*k_{21}a_1+a_2k_{21}^*a_1^* = 0 \tag{2.22}$$

Since the amplitude of $a_1$ and $a_2$ can be set arbitrarily, the coupling condition should satify the following,

$$k_{12} + k_{21}^* = 0 \tag{2.23}$$

and the value of $k_{12}$ and $k_{21}$ should be obtained from the energy conservation considerations. To evaluate the power transferred from the first resonator to the second resonator through the Mutual Inductance, equation (2.21) is can be calculated as

$$P_{21} = \frac{d|a_2|^2}{dt} = k_{21}a_1a_2^* + k_{21}^*a_1^*a_2 \tag{2.24}$$

From figure 2.4, power flowing through M can be expressed as

$$P_{21} = i_2M\frac{d(i_1 - i_2)}{dt} \tag{2.25}$$

Then, by intorducing complex current envelope quantities $I_1(t)$, $I_2(t)$, the current expression $i_1(t)$ can be defined as,

$$i_1(t) = \frac{1}{2}(I_1(t)e^{j\omega_1 t} + I_1^*(t)e^{-j\omega_1 t}) \tag{2.26}$$

and $i_2(t)$ can be defined similarly. By substituting $i_1(t)$ and $i_2(t)$ into (2.25), the transferred power can be rewritten as following,

$$P_{21} = \frac{1}{4}(I_2(t)e^{j\omega_2 t}+I_2^*(t)e^{-j\omega_2 t}) \left(\frac{d}{dt}(I_1(t)e^{j\omega_1 t} + I_1^*(t)e^{-j\omega_1 t} - I_2(t)e^{j\omega_2 t} + I_2^*(t)e^{-j\omega_2 t})\right) \tag{2.27}$$

From here $\left(\frac{d}{dt}I_1\right)e^{e\omega_1 t}$ are relatively much smaller than $j\omega I_1$, and can be ignored. Thus, equation (2.27) can be rewritten into (2.28)

$$P_{21} = \frac{1}{4}\left(j\omega_1 M I_1 I_2^* e^{j(\omega_1-\omega_2)t} - j\omega_1 M I_1^* I_2 e^{-j(\omega_1-\omega_2)t}\right) \tag{2.28}$$

Comparing (2.28) with (2.24), and defining $a_n = \sqrt{\frac{L_n}{2}}I_n e^{j\omega_n t}$, where $n = 1, 2$, the coupling coefficient can be derived as

$$k_{21} = \frac{j\omega_1 M}{2\sqrt{L_1 L_2}} \tag{2.29}$$

From (2.23), the complex number of $k_{21}$ can be derive as (2.30).

$$k_{21} = k_{12} = jk = \frac{j\omega M}{2\sqrt{L_1 L_2}} \tag{2.30}$$

where $\omega$ is the arithmetic mean of $\frac{\omega_1+\omega_2}{2}$ or the geometric mean of $\sqrt{\omega_1\omega_2}$ of resonant frequency of each of the resonators.

### 2.2.5 Full Wireless Power Transfer System

Figure 2.5 show the complete scheme of the wireless power transfer system. $Z_s$ presents the internal impedance of the power source and $H$ is the distance between the source and load coils.

Applying the aforementioned expression in previous sections, the full model of the system can be presented using CMT as follows,

$$\frac{da_1(t)}{dt} = j\omega_1 a_1(t) - (\Gamma_{ext1} + \Gamma_1)a_1(t) + jka_2(t) + \sqrt{2\Gamma_{ext1}}s_+(t) \tag{2.31}$$

$$\frac{da_2(t)}{dt} = j\omega_2 a_2(t) - \Gamma_2 a_2(t) + jka_1(t) \tag{2.32}$$

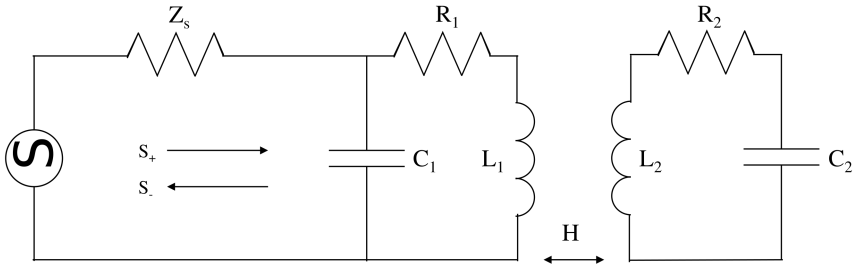


Figure 2.5: Complete Wireless Power Transfer Scheme

To express the full wireless power transfer system, the term of the load need to be introduced. Considering the load is defined by $|s_{+n}(t)|^2$ which is power ingoing to the object $n(n = 1, 2)$ and $|s_{-n}(t)|^2$ which is the outgoing power from the resonant object $n$, the full system can be written as (2.33).

$$\begin{aligned}
\frac{da_1(t)}{dt} &= j\omega_1 a_1(t) - (\Gamma_{ext1} + \Gamma_1)a_1(t) + jka_2(t) + \sqrt{2\Gamma_{ext1}}s_{+1}(t) \\
\frac{da_2(t)}{dt} &= j\omega_2 a_2(t) - (\Gamma_{ext2} + \Gamma_2)a_2(t) + jka_1(t) \\
s_1(t) &= \sqrt{2\Gamma ext1}a_1(t) - s_{+1}(t) \\
s_1(t) &= \sqrt{2\Gamma_{ext2}}a_2(t)
\end{aligned} \tag{2.33}$$

### 2.2.6 Finite-amount Power Transfer

Supposing there is no power source and load on the system, equation (2.33) changes into equation(2.34)

$$\begin{aligned}
\frac{da_1(t)}{dt} &= j\omega a_1(t) - \Gamma_1 a_1(t) + jka_2(t) \\
\frac{da_2(t)}{dt} &= j\omega a_2(t) - \Gamma_2 a_2(t) + jka_1(t)
\end{aligned} \tag{2.34}$$

where 1 and 2 denote the source coil and load coil. From here, (2.34) can be rewritten as

$$\dot{\vec{a}}(t) = A\vec{a}(t) \tag{2.35}$$

where $\dot{\vec{a}}$ is a vector which involves the the mode amplitude of the source and

the load coil. The matrix A can be define as,

$$A = \begin{bmatrix} j\omega_1 - \Gamma_1 & jk \\ jk & j\omega_2 - \Gamma_2 \end{bmatrix} \tag{2.36}$$

Eigen values of the system can be obtained by solving the characteristics equation of $det(A - sI) = 0$, which can be represented by following,

$$\begin{aligned} x_1 &= j\frac{\omega_1 + \omega_2}{2} - \frac{\Gamma_1 + \Gamma_2}{2} + j\sqrt{\left(\frac{\omega_1 - \omega_2}{2} - j\frac{\Gamma_1 - \Gamma_2}{2}\right)^2 + k^2} \\ x_2 &= j\frac{\omega_1 + \omega_2}{2} - \frac{\Gamma_1 + \Gamma_2}{2} + j\sqrt{\left(\frac{\omega_1 - \omega_2}{2} - j\frac{\Gamma_1 - \Gamma_2}{2}\right)^2 + k^2} \end{aligned} \tag{2.37}$$

thus,

$$\vec{a}(t) = \begin{bmatrix} a_1(t) \\ a_2(t) \end{bmatrix} = c_1 V_1 e^{x_1 t} + c_2 V_2 e^{e x_2 t} \tag{2.38}$$

where $c_1$ and $c_2$ are constants determined by the initial conditions and $V_1$,$V_2$ are the eigen vectors. The eigen vector can be calculated as (2.39)

$$\begin{aligned} V_1 &= \begin{bmatrix} -\frac{1}{k}\left(\frac{\omega_2 - \omega_1}{2} + \frac{\Gamma_2 - \Gamma_1}{2} - \Omega_0\right) \\ 1 \end{bmatrix} \\ V_2 &= \begin{bmatrix} -\frac{1}{k}\left(\frac{\omega_2 - \omega_1}{2} + \frac{\Gamma_2 - \Gamma_1}{2} + \Omega_0\right) \\ 1 \end{bmatrix} \end{aligned} \tag{2.39}$$

where

$$\Omega_0 = \sqrt{\left(\frac{\omega_1 - \omega_2}{2} - j\frac{\Gamma_1 - \Gamma_2}{2}\right)^2 + k^2} \tag{2.40}$$

Now, assuming that $t = 0$ the source coil has the energy of $|a_1(0)|^2$ and the energy contained at the source coil at the same time is $|a_2(0)|^2$. The resonant modes can be expressed as (2.41).

$$\begin{aligned} a_1(t) &= \left(a_1(0)\left(\cos(\Omega_0 t) + \frac{\Gamma_2 - \Gamma_1}{2\Omega_0 t}\sin(\Omega_0 t) - j\frac{\omega_2 - \omega_1}{2\Omega_0 t}\right) + a_2(0)\frac{jk}{\Omega_0}\sin(\Omega_0 t)\sin(\Omega_0 t)\right) \\ &\quad \cdot e^{j\frac{\omega_1 + \omega_2}{2}t} e^{-\frac{\Gamma_1 + \Gamma_2}{2}t} \\ a_2(t) &= \left(a_1(0)\frac{jk}{\Omega_0}\sin(\Omega_0 t) + a_2(0)\left(\cos(\Omega_0 t) - \frac{\Gamma_2 - \Gamma_1}{2\Omega_0 t}\sin(\Omega_0 t) + j\frac{\omega_2 - \omega_1}{2\Omega_0 t}\sin(\Omega_0 t)\right)\right) \\ &\quad \cdot e^{j\frac{\omega_1 + \omega_2}{2}t} e^{-\frac{\Gamma_1 + \Gamma_2}{2}t} \end{aligned} \tag{2.41}$$

In case where the load coil is identical to the source coil, $\omega_1 = \omega_2 = \omega_0$ , $\Gamma_1 = \Gamma_2 = \Gamma_0$ and $|a_2(0)|^2 = 0$ can be simplified to (2.42).

$$\begin{aligned} a_1(t) = &\quad a_1(0)\cos(kt)e^{j\omega_0 t}e^{-\Gamma_0 t} \\ a_2(t) = &\quad ja_1(0)\sin(kt)e^{j\omega_0 t}e^{-\Gamma_0 t} \end{aligned} \tag{2.42}$$

The energy transfer efficiency for finite-amount of power transfer is determined by,

$$\eta = \frac{|a_2(t)|^2}{|a_1(0)|^2} \tag{2.43}$$

### 2.2.7 Wireless Power Transfer with Source and Load

When the source coil is continuously connected to the power source and the load connected to the load coil through $\Gamma_{ext1}$ and $\Gamma_{ext2}$, and the excitation frequency is considered fixed and equal to $\omega$, the field amplitude is expressed as,

$$s_{+1}(t) = S_{+1}e^{j\omega t} \tag{2.44}$$

where the $S_{+1}$ is a constant determined by the amplitude of the incident wave. Then it is possible to express (2.33) into following,

$$\dot{\vec{a}}(t) = \begin{bmatrix} j\omega_1 - \Gamma_1 & jk \\ jk & j\omega_2 - \Gamma_2 \end{bmatrix} \vec{a}(t) + \begin{bmatrix} \sqrt{2\Gamma_{ext1}} \\ 0 \end{bmatrix} s_{+1}(t) \tag{2.45}$$

The transfer function of the system is derive by

$$\hat{g}(s) = \frac{\sqrt{2\Gamma_{ext1}}(s - j\omega_2 + \Gamma_2 - jk)}{s^2 - s(j\omega_1 + j\omega_2 + \Gamma_1 + \Gamma_2) - \omega_1\omega_2 - j\omega_1\Gamma_2 - j\omega_2\Gamma_1 + \Gamma_1\Gamma_2 + k^2} \tag{2.46}$$

The pole pair $s_{1,2}$ defined by

$$s_{1,2} = -\frac{\Gamma_1 + \Gamma_2}{2} + j\frac{\omega_1 + \omega_2}{2} \pm \frac{1}{2}\sqrt{(j(\omega_1 - \omega_2) + \Gamma_2 - \Gamma_1)^2 - 4k^2} \tag{2.47}$$

From the equations above, we can conclude that the poles of transfer function always contain negative real parts so (2.45) is considered Boundary Input

Boundary Output (BIBO) stable. BIBO stability and equation (2.44) together means that the response of a linear system $\vec{a}(t)$ will be at the same frequency $\omega$ as the input and can be presented as

$$a_{1,2}(t) = A_{1,2}e^{j\omega t} \tag{2.48}$$

The same discussion can be applied to $s_{-1,2}(t)$ and can be expressed as below.

$$s_{-1,2}(t) = S_{-1,2}e^{j\omega t} \tag{2.49}$$

Substituting the equation (2.48) and (2.49) into (2.33), we get the transmission coefficient $S_{21}$ (from the scattering matrix which be discussed later).

$$S_{21} = \frac{s_{-2}}{s_{+1}} = \frac{2jk\sqrt{\Gamma_{ext1}\Gamma_{ext2}}}{(\Gamma_1 + \Gamma_{ext1} + j\delta_1)(\Gamma_2 + \Gamma_{ext2} + j\delta_2) + k^2} = \frac{2jU\sqrt{U_1U_2}}{(1 + U_1 + jD_1)(1 + U_2 + jD_2) + U^2} \tag{2.50}$$

where,

$$\left.\begin{aligned} \delta_{1,2} &= \omega - \omega_{1,2} \\ D_{1,2} &= \frac{\delta_{1,2}}{\Gamma_{1,2}} \\ U_{1,2} &= \frac{\Gamma_{ext_{1,2}}}{\Gamma_{1,2}} \\ U &= \frac{k}{\sqrt{\Gamma_1\Gamma_2}} \end{aligned}\right\} \tag{2.51}$$

Similarly, the reflection coefficient $S_{11}$ can be determined as,

$$S_{11} = \frac{(\Gamma_1 - \Gamma_{ext1} + j\delta_1)(\Gamma_2 + \Gamma_{ext2} + j\delta_2) + k^2}{(\Gamma_1 + \Gamma_{ext1} + j\delta_1)(\Gamma_2 + \Gamma_{ext2} + j\delta_2} = \frac{(1 - U_1 + jD_1)(1 + U_2 + jD_2) + U^2}{(1 + U_1 + jD_1)(1 + U_2 + jD_2) + U^2} \tag{2.52}$$

The maximum transmission efficiency can obtained from (2.50) to (2.53).

$$\eta = |S_{21}|^2 \tag{2.53}$$

## 2.3 Wireless Power Transfer by Equivalent Circuit Theory

After the Coupled Mode Theory of electromagnetism is introduced in early 1950's, the theory undergo alot of development. The current theory is suitable for analyzing the energy exchange process between two resonators. However the CMT concepts are still obscure.

Another method to model wireless power transmission scheme is by the equivalent circuit theory and the parameter of the scheme can be analyzes using the two-port network theory. Depending on the intended purpose, the two-port network can be characterized using equivalent circuit parameters, such as the transfer matrix, impedance matrix or the scattering matrix. As mentioned on the section before hand, the network matrices can also be represented using the definitions from the Coupled Mode Theory.

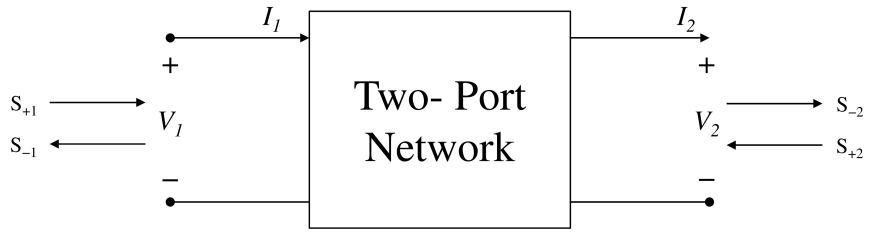


Figure 2.6: Two-Port Network

Figure 2.6 shows the two-port network sceheme. The impedance matrix and the scattering matrix can be expressed using (2.54).

$$\begin{bmatrix} V_1 \\ I_1 \end{bmatrix} = \underbrace{\begin{bmatrix} A & B \\ C & D \end{bmatrix}}_{\text{transfer matrix}} \begin{bmatrix} V_2 \\ I_2 \end{bmatrix}; \begin{bmatrix} V_1 \\ V_2 \end{bmatrix} = \underbrace{\begin{bmatrix} Z_{11} & Z_{12} \\ Z_{21} & Z_{22} \end{bmatrix}}_{\text{impedance matrix}} \begin{bmatrix} I_1 \\ -I_2 \end{bmatrix} \tag{2.54}$$

where $V_1$ and $V_2$ are the input and output voltages of the network and $I_1$ and $I_2$ are the input and output current of the network.Scattering matrix related to

the ingoing $s_{+1,2}$ and outgoing $s_{-1,2}$ waves of the network.

$$\begin{bmatrix} s_{-1} \\ s_{-2} \end{bmatrix} = \underbrace{\begin{bmatrix} S_{11} & S_{12} \\ S_{21} & S_{22} \end{bmatrix}}_{\text{scattering matrix}} \begin{bmatrix} s_{+1} \\ s_{+2} \end{bmatrix} \tag{2.55}$$

Usually in electronic circuit analysis, impedance and transfer matrices are used, However when the frequency becomes higher, the coefficient measurement becomes more complicated. Hence the scattering matrix is more preferred due to the existence of network analyzer which are able to measure the scattering matrix parameters over wide range of frequencies. Using this two-port network system concept, it is possible to calculate the power transfer between power source and the load in wireless power transfer system. Figure 2.7 shows the two-port network when the source and load side is attached.

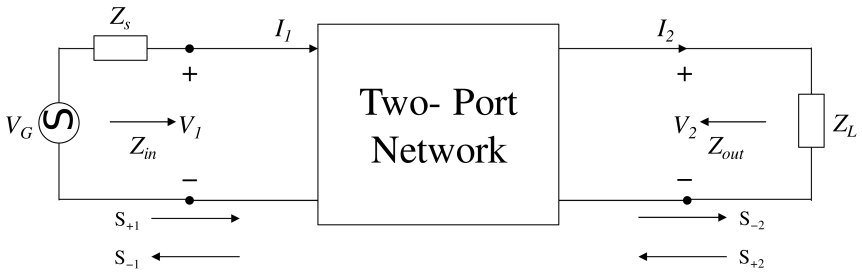


Figure 2.7: Two-Port Network Connected to Source and Load

Based on the scattering matrix analysis [30], the expression for the voltage and current in terms of the wave variable can be presented as,

$$\begin{aligned} V_1 &= \sqrt{Z_s}(s_{+1} + s_{-1}),\ V_2 &&= \sqrt{Z_s}(s_{+2} + s_{-2}) \\ I_1 &= \frac{1}{\sqrt{Z_s}}(s_{+1} - s_{-1}),\ I_2 &&= \frac{1}{\sqrt{Z_s}}(s_{+2} - s_{-2}) \end{aligned} \tag{2.56}$$

where $Z_s$ is the internal impedance of the source (normally is predetermined to be 50Ω), Considering the above equation, the scattering matrix can be defined as below.

$$\begin{aligned} V_1 &= Z_{in} I_1 \\ V_2 &= Z_L I_2 \end{aligned} \iff \begin{aligned} s_{-1} &= \Gamma_{in} s_{+1} \\ s_{-2} &= \Gamma_L s_{+2} \end{aligned} \tag{2.57}$$

where $Z_{in}$ is the input impedance of the network and $\Gamma_{in}$, $\Gamma_L$ are the reflection coefficients given by the following equations.

$$\begin{aligned} \Gamma_{in} &= \frac{Z_{in} - Z_s}{Z_{in} + Z_s} \\ \Gamma_L &= \frac{Z_L - Z_s}{Z_L + Z_s} \end{aligned} \tag{2.58}$$

From equation (2.56)-(2.58), it is possible to define the reflection coefficients in terms of the scattering matrix parameters.

$$\Gamma_{in} = S_{11} + \frac{S_{12}S_{21}\Gamma_L}{1 - S_{22}\Gamma_L} \tag{2.59}$$

Based from [30], reversing the roles of power source and load, we get two more reflection coefficients.

$$\Gamma_{out} = \frac{Z_{out} - Z_s}{Z_{out} + Z_s}\Gamma_G = \frac{Z_G - Z_s}{Z_G + Z_s} \tag{2.60}$$

where $Z_{out}$ is the output impedance. And this reflection coefficients depends on the scattering matrix parameters of

$$\Gamma_{out} = S_{22} + \frac{S_{12}S_{21}\Gamma_G}{1 - S_{11}\Gamma_G} \tag{2.61}$$

The efficiency of the wireless power transfer system can be obtained through $P_{in}$ (input power, coming into the two-port network from the power source) and $P_{out}$ (output power, going out from the two-port network towards the load). For the system shown in figure 2.7, the input power and out power can be defined as,

$$\begin{aligned} P_{in} &= \frac{1}{2}\frac{|V_G|^2 R_{in}}{|Z_{in} + Z_G|^2} \\ P_L &= \frac{1}{2}\frac{|V_G|^2 R_L |Z_{21}|^2}{|(Z_{11} + Z_G)(Z_{out} + Z_L|^2} \end{aligned} \tag{2.62}$$

where $R_{in} = Re(Z_{in})$ and $R_L = Re(Z_L)$. From (2.62), the optimal condition for maximum power delivery from the power source is

$$Z_{in} = Z_G^* \tag{2.63}$$

and similarly the maximum power can be output on the load side when

$$Z_L = Z_{out}^* \tag{2.64}$$

The power transfer efficiency can be expressed in terms of S-parameters using the following

$$\eta_1 = \frac{(1 - |\Gamma_G|^2)\,|S_{21}|^2\,(1 - |\Gamma_L|^2)}{|\,(1 - S_{11}\Gamma_G)\,(1 - S_{22}\Gamma_L) - S_{12}S_{21}\Gamma_G\Gamma_L|^2} \tag{2.65}$$

Here, when the source impedance matches the load impedance, the reflected coefficient could be represented as,

$$\Gamma_L = \Gamma_G = 0 \text{ and } \Gamma_{in} = S_{11}\ ,\ \Gamma_{out} = S_{22} \tag{2.66}$$

Substituting (2.66) into (2.65) the efficiency formula can be simplified into (2.67).

$$\eta_1 = |S_{21}|^2 \tag{2.67}$$

# Chapter 3

# The 13.56 MHz Antenna Design

## 3.1 Helical Coil

In previous research, wireless power transfer using resonant coil has been widely discussed. For example in [10], wireless power transfer between coil at distance of 2 meters with maximum efficiency of 40% was reported. In this paper, an air-core inductor or helical coil is choosen as the resonator of the wireless power trasnfer system. At high frequency, the behaviour of the inductor is very different from that at low frequency. Aside from the skin effect and proximity effect, the parasitic capacitance of the windings is also cannot be neglected at high fequency. In this chapter, the method to evaluate the self-inductance, parasitic capacitance and resistance of the helical coil inductor is presented. The modelling of the helical coil antenna that will be used in this research is based on the formalism evaluated in this chapter.

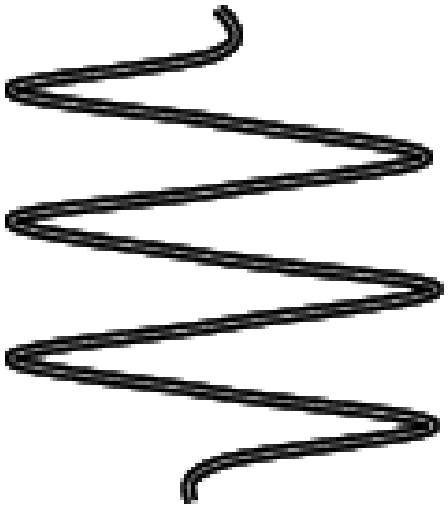

Figure 3.1: Helical Open Coil

Figure 3.1 shows the non loaded helical coil antenna diagram. Based on [16], the performance of the antenna depends on the quality factor of the helical coil. And the quality factor evaluation are often starts from the calculation of inductance of helical coil. At low frequency, the concept of lumped indutance is applicable where the length of the wire of the helical coil is relatively small compared to the wavelength of the frequency. However at high frequency, these

will be a phase difference between the waves from the output terminal antenna and the waves that come into the input terminal of the antenna. In order to evaluate the inductance of the antenna at high frequency, two considerations must be taken into account: the external inductance due to the magnetic energy stored in the surrounding medium and the internal inductance due to the magnetic energy inside the coil itself.

### 3.1.1 Self-Inductance Evaluation

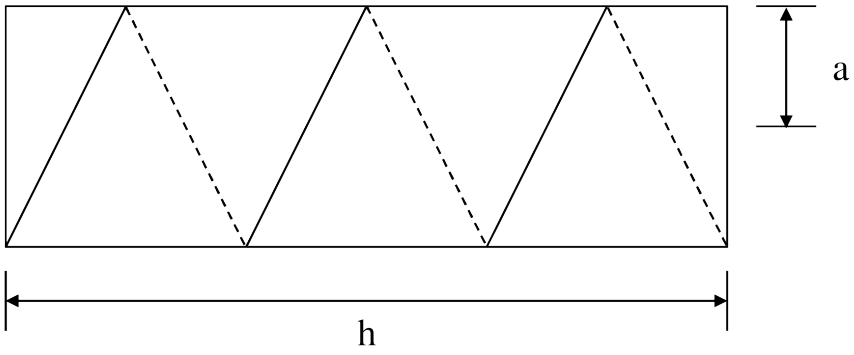


Figure 3.2: Current-Sheet Inductor

A current-sheet inductor (shown in figure 3.2 ) is usually used to represent the analysis of inductance. This is the representation when the conducting wire of the solenoid coil is infinately thin (one layer) and the spacing between the turns is non-existance. This coil is has the advantage of uniform magnetic field distribution along the coils length. If all of the assumptions are satisfied, the inductance of this coil can be expressed as (3.1):

$$L_s = \frac{\mu\pi(2a)^2N^2}{4h} \tag{3.1}$$

where $a$ is the radius of the coil, $N$ is the number of turns, $h$ is height of the helical coil and $\mu$ is the magnetic permeability. In this case, since the core is air-core, the magnetic permeability reduces to $\mu_0$.

Since current-sheet inductor is a theoretical model, few modifications is needed to use the model formula as the real inductors evaluation. The first modification

is the frequency independent modification using field non-uniformity correction coefficient ($k_f$), a self-induction correction coefficient for round wire ($k_s$) and the mutual inductance correction coefficient for winding wire ($k_m$).

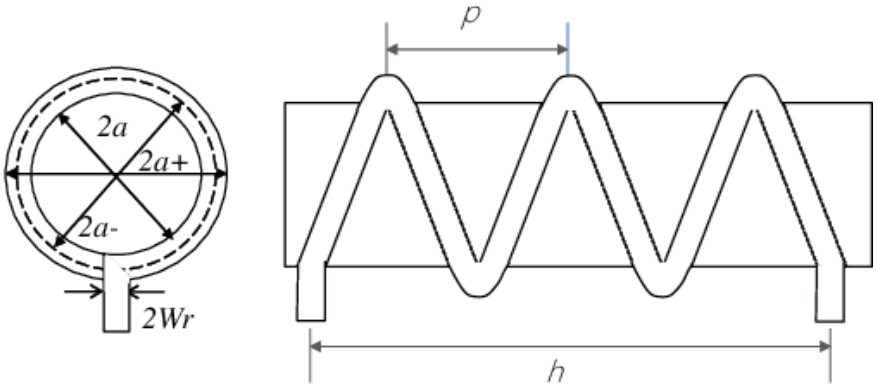


Figure 3.3: Finite Size Inductor using Round Wire

To depict the real helical coil, the wire form should have some finite size (round wire with wire radius $W_r$ and height) and the spacing between the turn is non-zero (turn to turn pitch $p$ exists). When the coil length is comparable to its diameter, the uniform field distribution assumption will no longer be valid. To consider about the non-uniformity, a coefficient $k_f$ is introduced in 1909 by H. Nagaoka [28].

$$k_f = \frac{h}{\pi a}\left[\frac{\left(\ln\frac{8a}{h}-\frac{1}{2}\right)\left[1+0.383901\left(\frac{h}{2a}\right)^2+0.017108\left(\frac{h}{2a}\right)^4\right]}{1+0.258952(\frac{h}{2a})^2+0.093842(\frac{h}{2a})^2+0.002029(\frac{h}{2a})^4-0.000801(\frac{h}{2a})^6}\right] \tag{3.2}$$

Using this modification, equation (3.1) can be rewritten as

$$L_s = \frac{\mu\pi(2a)^2N^2}{4h}k_f \tag{3.3}$$

In real helical coils, the coefficient to consider about the shape of the conductor and the effect of the mutual inductance between the adjacent turn of the coils is also important. E.B Rosa [31] presented a new equation with considerations of this two effects in 1916.

$$L = L_s - \frac{\mu N 2a}{2}(k_s + k_m) \tag{3.4}$$

where,

$$k_s = \frac{3}{2} - \ln \frac{p}{W_r}$$
$$k_m = ln(2\pi) - \frac{3}{2} - \frac{\ln(N)}{6N} - \frac{0.33084236}{N} - \frac{1}{120N^3} + \frac{1}{504N^5} - \frac{0.0011923}{N^7} + \frac{0.0005068}{N^9} \quad (3.5)$$

where $\mu$ in this case is considered as air-core, and can be considered $\mu_0$.

### 3.1.2 Parasitic Capacitance Evaluation

When air core inductor is operated at high frequency, the behaviour of the parasitic capacitance between the windings cannnot be neglected as it will significantly effect the inductance of the coil and the resonating frequency. In this section, the analytical approach to evaluate the parasitic capacitance in helical coil is presented based on [9]. In this research, a single wire wound is used as a single layer solenoid to reduce the turn-to-turn stray capacitance between the solenoid layers. The coil is also air-cored to prevent the turn-to-core stray capacitance. The distance between the turns is spaced largely enough to avoid high turn-to-turn capacitance of the coil.

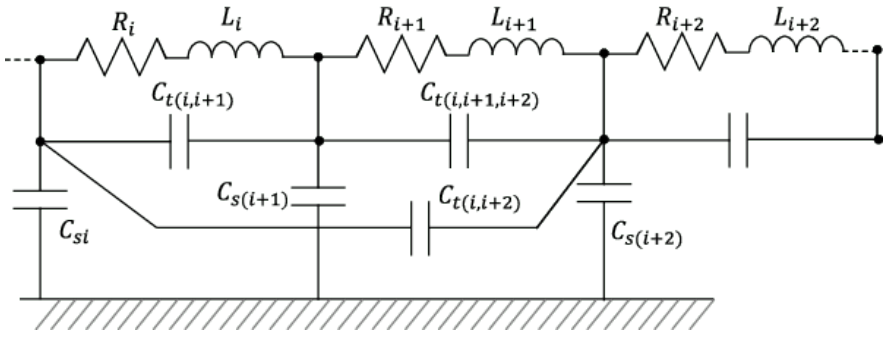


Figure 3.4: HF Equivalent Circuit of Single Layer Air-Core Helical Coils with Shield

Figure 3.4 illustrates the detailed HF equivalent circuit for a single-layer air-core helical coil. The parameters are related to every turn or pair turns of the coil windings. With single layer air-core helical coils that has $N$ number of turns as

shown in figure 3.4, the stray capacitance that exists in the circuit is considered to be:

- turn-to-turn capacitance, $C_{t(i,j)} i, j = 1, 2, \ldots, N; i \neq j$;
- turn-to-shield capacitance, $C_{si}, i = 1, 2, \ldots, N$.

From figure 3.4, $R_i$ and $L_i$ are the windings resistance and theself-inductance of the $i$th turn of the helical coils respectively. Due to the symmetries of the windings,

$$\begin{aligned} C_{t(i,i+1)} = C_{t(i+1,i+2)} = \cdots = C_{tt} \\ C_{si} = C_{s(i+1)} = \cdots = C_{ts} \\ R_i = R_{i+1} = \cdots = R_t = \frac{R_p}{N} \end{aligned} \tag{3.6}$$

where $R_p$ is the total internal resistance of the helical coil.

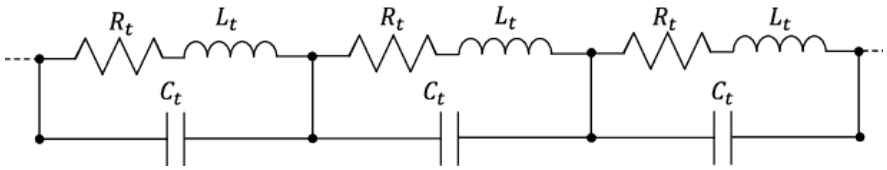


Figure 3.5: HF Equivalent Circuit of Single Layer Air-Core Helical Coil without Shield and Fringe Effect

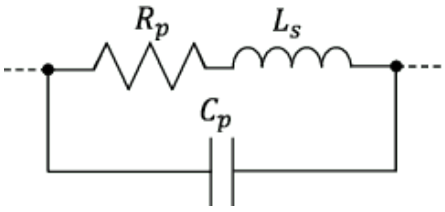


Figure 3.6: Simplified HF Equivalent Circuit of Single Layer Air-Core Helical Coil without Shield

When the uniform voltage distribution along the windings can be assumed, the HF equivalent circuit can be deduced into simpler version of figure 3.5. In this case, the helical coil is placed far enough from the shield to be influenced

and the fringe effect are negligible. If the helical coil is designed to be symmetry, the self-inductance and capacitance effect the between the turns can be justified to be the same. Each turn have the same self-inductance, $L_t = L_s/N$ where $L_s$ is the total self-indutance of the coil. The $C_t$ in figure 3.5 represents the equivalent capacitance between two corresponding points of any pair of adjacent turns.

From equivalent circuit in figure 3.5 , the HF model of the helical coil can be simplified into figure 3.6. Here the $L_s$, $C_p$ and $R_p$ can be expressed as:

$$\left.\begin{aligned} L_s &= NL_t \\ R_p &= NR_t \\ C_p &= C_t \end{aligned}\right\} \tag{3.7}$$

For the given circuit in figure 3.6, the overall parasitic capacitance $C_p$ is given in (3.7). Typically the stray capacitance between the non-adjacent turns is smaller than the adjacent turn. By neglecting the non-adjacent turn capacitance, the equivalent turn capacitance $C_t$ can be calculated and can be reduced to turn-to-turn capacitance, $C_{tt}$. Since the turn to shield capacitance can also be neglected, the total overall stray capacitance $C_{AB}$ in figure 3.6 can be expressed as,

$$C_{AB} = \frac{C_{tt}}{N-1} \tag{3.8}$$

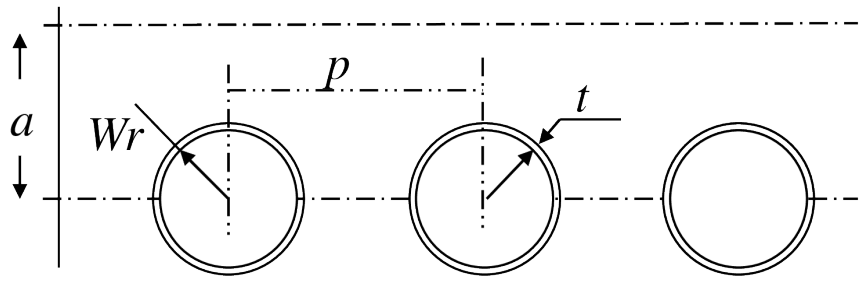


Figure 3.7: Cross-sectional View of Helical Coil And Shield

Figure 3.7 shows the cross-sectional view of helical coil and shield. We can assume that the capacitance between two adjacent turns $C_{tt}$ can be calculated from the formula for the capacitance per unit length of two infinitely long straight parallel conductors placed in homogeneous medium. When the thickness $t$ of the

insulating material of the conductor is relatively smaller than the air gap distance between the turns, $g = (p - 2W_r)$, the analytical expression to derive the turn-to-turn capacitance of circular cross-section wire is [44],

$$C_{tt} = \frac{\pi^2 2a\epsilon_0}{\ln(p/2W_r + \sqrt{(p/2W_r)^2 - 1})} \text{for } t \ll p - 2W_r \tag{3.9}$$

where $p$ is the winding pitch of the helical coil and $W_r$ is wire radius, respectively.

When the thickness $t$ of the insulation coating of relative permittivity $\epsilon_{W_r}$ is comparable to the air gap, the following expression can be derived assuming to the radial field in the insulating coating.

$$C_{tt} = \frac{\pi^2 2a\epsilon_0}{\ln(F + \sqrt{F^2 - (1 + t/W_r)^{2/\epsilon_{W_r}}})} \tag{3.10}$$

where

$$F = \frac{p/2W_r}{(1 + t/W_r)^{1/\epsilon_{W_r}}} \tag{3.11}$$

When the effect of the shield to the helical coil turns cannot be neglected, the turn-to-shield capacitance, $C_{ts}$ can be evaluated by using the following expression.

$$C_{ts} = \frac{\pi^2 2a\epsilon_0}{\ln(h_s/W_r + \sqrt{(h_s/W_r)^2 - 1})} \tag{3.12}$$

where $h_s$ is the distance between the shield and the coil winding.

### 3.1.3 Resistance Evaluation

From [25], four components of resistance is needed to represent the total resistance in the helical coils, i.e the $R_{dc}$ components, the skin effect components ($\Theta$), the proximity effect component ($\psi$) and for very high frequencies, the radiated resistance component ($R_r$) must be added.

$$\begin{aligned} R_p &= R_{dc}\Theta\psi + R_r, \text{where,} \\ R_r &= \sqrt{\frac{\mu_0}{\epsilon_0}} \left( \frac{\pi}{12} N^2 \left( \frac{a\omega}{c} \right)^4 + \frac{2}{3\pi^2} \left( \frac{\omega h}{c} \right)^2 \right) \end{aligned} \tag{3.13}$$

Table 3.1: Proximity Factor $\psi$

| $p/2W_r$ \ $h/2a$ | 1 | 1.111 | 1.25 | 1.43 | 1.66 | 2 | 2.5 | 3.33 | 5 | 10 |
|---|---|---|---|---|---|---|---|---|---|---|
| 0 | 5.31 | 3.37 | 2.74 | 2.12 | 1.74 | 1.44 | 1.20 | 1.16 | 1.07 | 1.02 |
| 0.2 | 5.45 | 3.84 | 2.83 | 2.20 | 1.77 | 1.48 | 1.29 | 1.19 | 1.08 | 1.02 |
| 0.4 | 5.64 | 3.99 | 2.97 | 2.28 | 1.83 | 1.54 | 1.33 | 1.21 | 1.08 | 1.03 |
| 0.6 | 5.80 | 4.11 | 3.10 | 2.38 | 1.89 | 1.60 | 1.38 | 1.22 | 1.10 | 1.03 |
| 0.8 | 5.80 | 4.17 | 3.20 | 2.44 | 1.92 | 1.64 | 1.42 | 1.23 | 1.10 | 1.03 |
| 1 | 5.55 | 4.10 | 3.17 | 2.47 | 1.94 | 1.67 | 1.45 | 1.24 | 1.10 | 1.03 |
| 2 | 4.10 | 3.36 | 2.74 | 2.32 | 1.98 | 1.74 | 1.50 | 1.28 | 1.13 | 1.04 |
| 4 | 3.54 | 3.05 | 2.60 | 2.27 | 2.01 | 1.78 | 1.54 | 1.32 | 1.15 | 1.04 |
| 6 | 3.31 | 2.29 | 2.60 | 2.29 | 2.03 | 1.80 | 1.56 | 1.34 | 1.16 | 1.04 |
| 8 | 3.20 | 2.90 | 2.62 | 2.34 | 2.08 | 1.81 | 1.57 | 1.34 | 1.165 | 1.04 |
| 10 | 3.23 | 2.93 | 2.65 | 2.27 | 2.10 | 1.83 | 1.58 | 1.35 | 1.17 | 1.04 |
| $\infty$ | 3.41 | 3.11 | 2.815 | 2.51 | 2.22 | 1.93 | 1.65 | 1.395 | 1.19 | 1.05 |

where, $c$ is the speed of light, $R_{dc} = \rho l/(\pi W_r^2)$ and $\Theta = W_r^2/(2W_r\delta_i - \delta_i^2)$ respectively. And $l$ is the length of wire and is equal to $l = \sqrt{(\pi 2a)^2 + h^2}$.

Eventhough the $R_{dc}$and$\Theta$ can be derived, the resistance due to the proximity effect factor is not easily derived. In his experiments, Medhurst formed a table of coefficient $\psi$, based on the geometric property of coils (Table 3.1).

## 3.2 Antenna Design

The coupling system which is called antenna is the importance part of WPT system because it makes power transfer system become wirelessly. It also determines the transfer distance and efficiency of system. It can be designed in many shape, structure and configuration ([4, 19, 26, 33, 34, 41, 43]). With magnetic coupling resonance theory, coupling system can be divided into normal CMR (Fig. 3.8(a)) and SCMR (Fig. 3.8(b)). In normal CMR, transferring side or receiving side consist of resonant coil and external capacitor in serial. The combination of capacitor

and inductance of resonance coil is the resonance circuit.

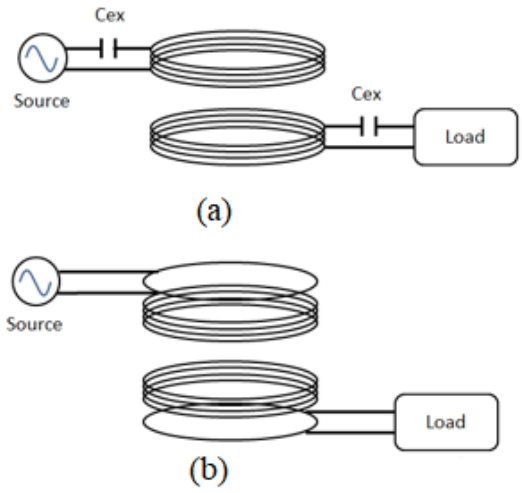


Figure 3.8: Configuration of coupling system. (a) Coupled Magnetic Resonance (CMR) and (b) Strongly Coupled Magnetic Resonance (SCMR)

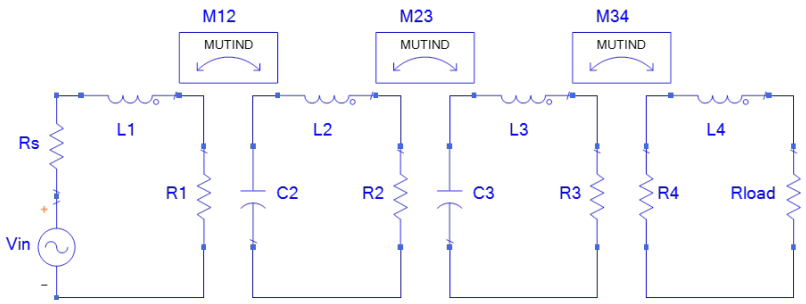


Figure 3.9: Equivalent circuit of the SCMR

The structure of SCMR is much different from CMR. The SCMR structure consists of four coils. They are divided into driver side and load side: the ring and the resonance coil. The capacitance between coils, the parasitic capacitance inside the coils and the inductance of coils make a resonance circuit. The equivalent circuit of SCMR is shown in Fig. 3.9. The Vs and Rs are the internal parameters of the power source. $R_1$ and $L_1$, $R_2$ and $L_2$, $R_3$ and $L_3$, $R_4$ and $L_4$ are the internal resistor and inductance of transmitting ring, transmitting coil, receiving

coil and receiving ring, respectively. The internal and parasitic capacitance of transmitting coil and receiving coil is $C_2$ and $C_3$, respectively. The main mutual inductances are $M_{12}$, $M_{23}$ and $M_{34}$. The resonance occurres between coils if there private resonance frequency is matching.

### 3.2.1 Finite Element Analysis

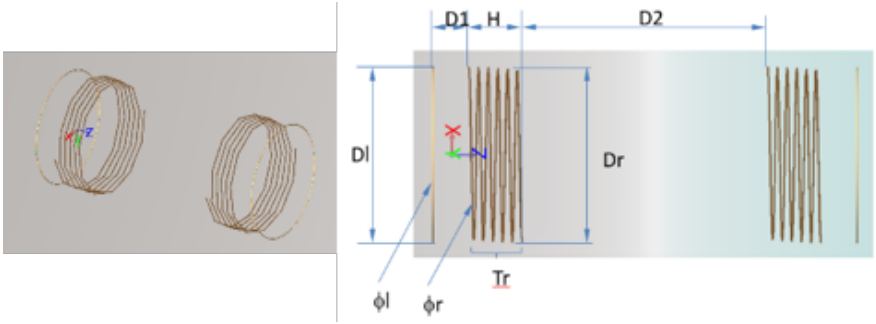


Figure 3.10: 3D Model of the antenna

The antenna can be analyzed by s-parameter method. With this method, the antenna is replaced by state with two ports. The source side port is P1 and the load side is P2. The transmission S21 is exported by finite element analysis (FEA) or measured by the vector network analyzer (VNA). The efficiency of coupling system is defined by equation:

$$\eta = |S_{21}|^2 \tag{3.14}$$

In order to achieve the resonant frequency and high efficiency of the antenna, we investigate the effect of mechanical parameters by simulation. In this case, the 3D model of coupling system is built and FEA is used to get the simulation result. The 3D model is shown in Fig. 3.10. The basic model which parameters in Table 3.2 is firstly simulated. After that, the parameter which is investigated is changed around the first parameter. The results are shown in Fig. 3.11.

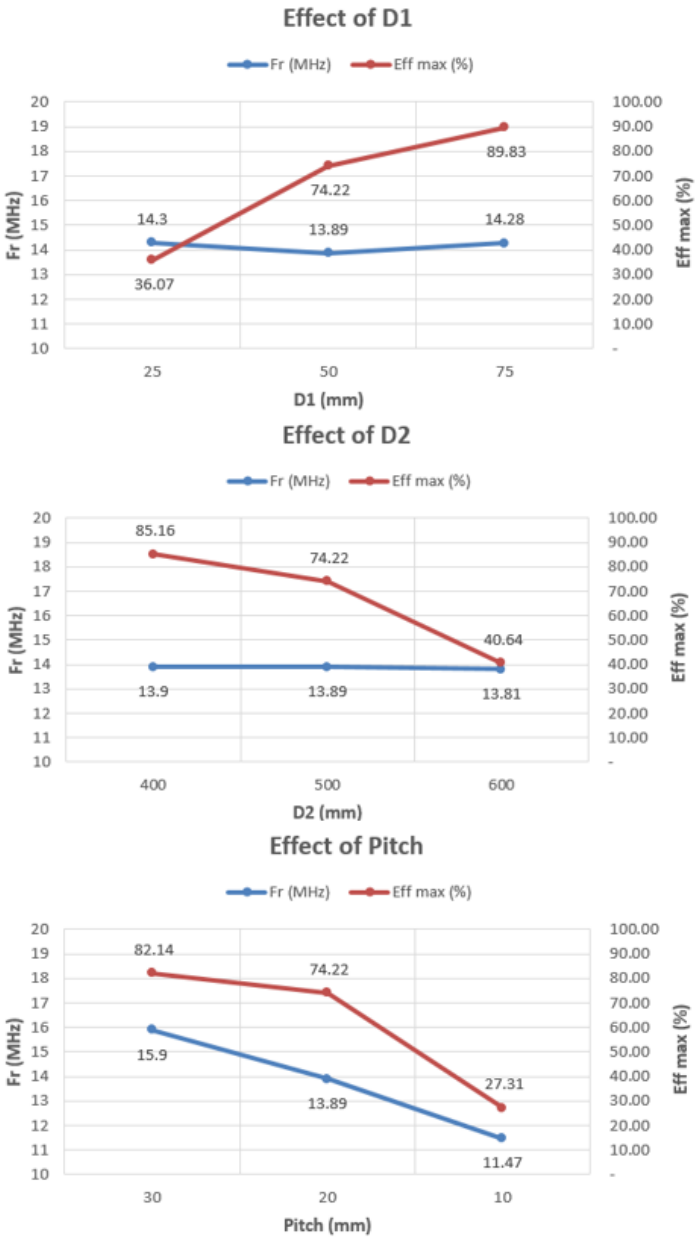


Figure 3.11: The effect of antenna parameters to the resonance frequency and maximum efficiency

Table 3.2: The parameters of basic model

| $\phi$l (mm) | $\phi$r (mm) | Tr | Hr (mm) | Pitch (mm) | D1 (mm) | D2 (mm) |
|---|---|---|---|---|---|---|
| 3 | 3 | 5 | 100 | 20 | 50 | 500 |

### 3.2.2 Optimized Design

The optimization is produced by the Finite Element Analysis (FEA). The optimized result of the design and parameters of the system are shown in Table 3.3 and Fig. 3.12. The driver side and load side are designed with the same parameters. The results show that the resonant frequency is 13.56 Mz. The efficiency is calculated from the s-parameter of FEA model by equation (3.14). The maximum calculated efficiency is 91.2%. The efficiency of the antenna verus the transfer distance is shown in Fig. 3.13.

The physical version of the antenna is constructed. It is shown in the Fig. 4.14. The block diagram of the experiment is shown in Fig. 3.14. The amplifier gererates the 13.56 MHz sine wave and the precious power. The antenna transfer the power wirelessly. The ouput of the antenna is connected to the 50 ohm resistor. The transfer efficiency of the antenna is shown in Fig. 3.15. The antenna is also verified in the wireless power transfer system (Fig. 4.14).

Table 3.3: The parameters of optimized design

| Name | Value | Description |
|---|---|---|
| Fres | 13.56MHz | Resonance Frequency |
| Dtf | 550 mm | Transfer Distance |
| Dmis | 0 mm | Misalignment |
| D12 | 120 mm | Distance between the link coil and the resonance coil |
| Dres | 400 mm | Diameter of the resonance coil |
| Dlink | 350 mm | Diameter of link coil |
| Dw | 3.2 mm | Diameter of copper wire |
| Pitch | 20 mm | Pitch of the resonance coil |
| Nt | 5.18 | Number of turns of the resonance coil |
| Eff | 91.2% | Efficiency of the antenna |

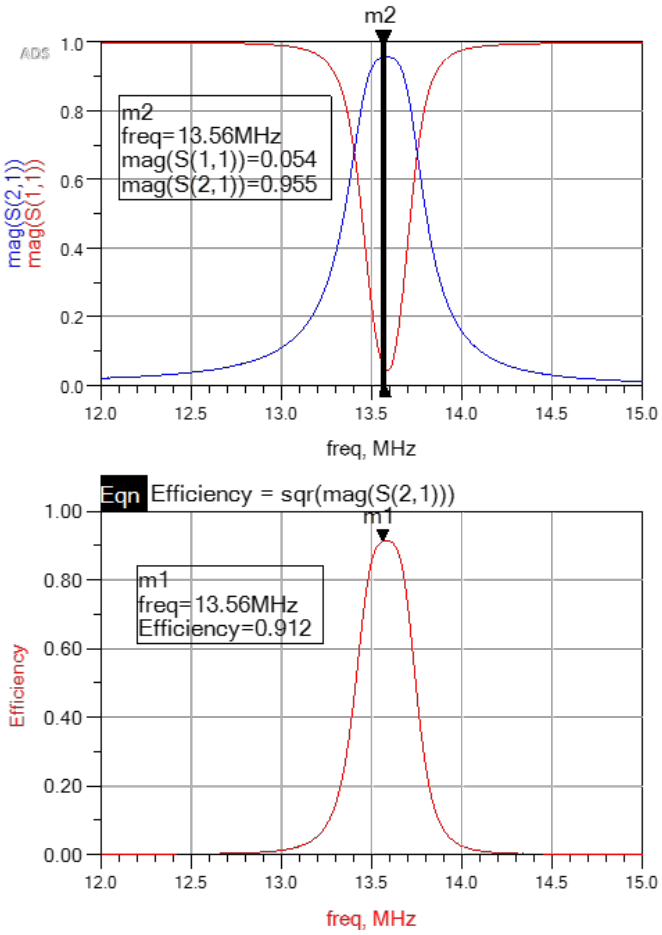


Figure 3.12: The S-parameter of the simulation result

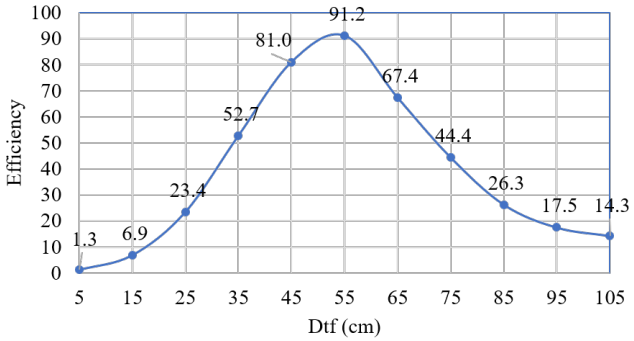


Figure 3.13: The efficiency verus the transfer distance

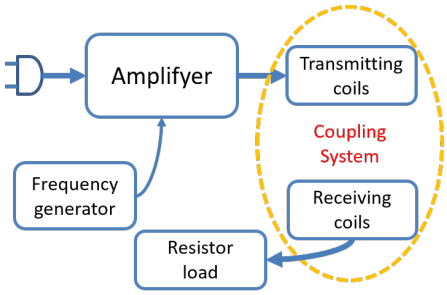


Figure 3.14: The block diagram of the experimental system

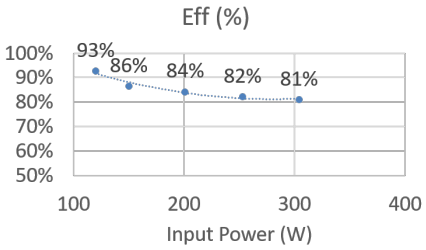


Figure 3.15: The efficiency of the antenna in experiment

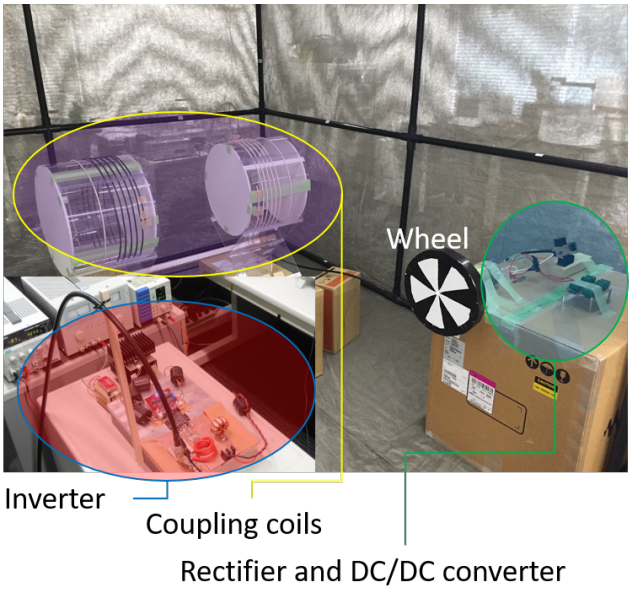


Figure 3.16: The antenna in the WPT system

# Chapter 4

# Antenna Efficiency Improvement For The Wireless Dynamic Charging System

## 4.1 Dynamic charging problem and solution

The dynamic wireless charging (DWC) is the development of the static wireless charging (SWC). It reduces the capacity of the EV's battery. The DWC can be configured by setting some SWC system continuously [1, 8, 13, 14, 36, 45]. But the problem is the interaction of each other and the high cost of numbers of the transmitter. This section shows the solution to improve the antenna's efficiency in charging area. Therefore, the numbers of transmitter can be reduced.

### 4.1.1 The problem analysys

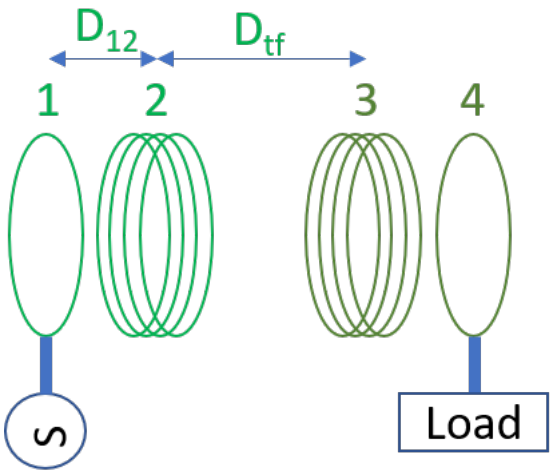


Figure 4.1: The strongly coupled magnetic resonance

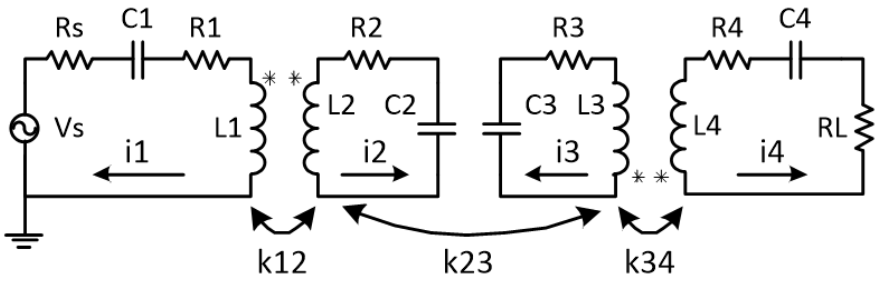


Figure 4.2: The equivalent circuit of four-coil system

The typical model of four-coil power transfer system is shown in Fig. 4.1. The detail already is descripted in section 3. In order to clearly explain the issue of the system, the represented circuit is shown in Fig. 4.2. Normally, the AC power supply can be either a power amplifier of a vector network analyzer (VNA) which is useful to measure a transmission and reflection ratio of the system. Therefore, the value of $R_S$ and $R_L$ is $50\omega$. The circuit model offers a convenient way to analyze the system's characteristic. By choosing the currents in each circuit as in Fig. 4.2 and applying circuit Kirchhoff's Voltage Law to the system, a relationship between currents and voltages can be captured as equation (4.1).

$$\begin{bmatrix} V_S \\ 0 \\ 0 \\ 0 \end{bmatrix} = \begin{bmatrix} Z_1 & j\omega M_{12} & 0 & 0 \\ j\omega M_{12} & Z_2 & -j\omega M_{23} & 0 \\ 0 & -j\omega M_{23} & Z_3 & j\omega M_{34} \\ 0 & 0 & j\omega M_{34} & Z_4 \end{bmatrix} \begin{bmatrix} i_1 \\ i_2 \\ i_3 \\ i_4 \end{bmatrix} \tag{4.1}$$

The $Z_i$ (with $i = 1 \sim 4$) are indicated as:
$Z_1 = R_S + R_1 + j(\omega L_1 - \frac{1}{\omega C_1})$
$Z_2 = R_2 + j(\omega L_2 - \frac{1}{\omega C_2})$
$Z_3 = R_3 + j(\omega L_3 - \frac{1}{\omega C_3})$
$Z_4 = R_L + R_4 + j(\omega L_4 - \frac{1}{\omega C_4})$

It is clearly seen that the voltage across the load is equal to $V_L = -i_4 R_L$ and the relationship between the voltages of the source and load is given as $V_L/V_S$. As the content of section 2, the s-parameter is a suitable candidate to analyze a figure of merit of this system. $S_{21}$ is determining of power transfer efficiency which is given by $|S_{21}|^2$. The parameter of $S_{21}$ is calculated by equation (4.2) [32].

$$S_{21} = 2\frac{V_L}{V_S}\sqrt{\frac{R_S}{R_L}} \tag{4.2}$$

$$S_{21} = \frac{j2\omega K_{12}K_{23}K_{34}L_2L_3\sqrt{L_1L_4R_SR_L}}{Z_1Z_2Z_3Z_4 + K_{12}^2L_1L_2Z_3Z_4\omega^2 + K_{23}^2L_2L_3Z_1Z_4\omega^2 + K_{34}^2L_3L_4Z_1Z_2\omega^2 +} \tag{4.3}$$

$$\overline{+K_{12}^2K_{34}^2L_1L_2L_3L_4\omega^4}$$

## 4. ANTENNA EFFICIENCY IMPROVEMENT FOR THE WIRELESS DYNAMIC CHARGING SYSTEM

The quality factor which appreciates how well the resonator can oscillate is defined as:

$Q_i = \frac{1}{R_i}\sqrt{\frac{L_i}{C_i}} = \frac{\omega_i L_i}{R_i} \quad \Leftrightarrow \quad \omega_i Li = R_i Q_i; \quad i = 1 \sim 4$

When the resonance takes place:

$\omega_i = \omega_0$

$Z_1 = R_S + R_1 \approx R_S$

$Z_2 = R_2$

$Z_3 = R_3$

$Z_4 = R_L + R_4 \approx R_L$

$$|S_{21}| = \frac{2K_{12}K_{23}K_{34}Q_2Q_3\sqrt{Q_1Q_4}}{1 + K_{12}^2Q_1Q_2 + K_{23}^2Q_2Q_3K_{34}^2Q_3Q_4 + K_{12}^2K_{34}^2Q_1Q_2Q_3Q_4} \tag{4.4}$$

The variation of $|S_{21}|$ is similar the line in depends on the Fig. 4.4. It depends on the variation of $K_{23}$. With the variation of $K_{23}$ in the dynamic wireless charging system, $|S_{21}|$ or efficiency $\eta$ is maximum when:

$$\frac{d|S_{21}|}{dK_{23}} = 0 \Leftrightarrow K_{23}^* = \sqrt{\frac{(1 + K_{12}Q_1Q_2)(1 + K_{34}^2)Q_3Q_4}{Q_2Q_3}} \tag{4.5}$$

$$|S_{21}|_{max} = \frac{K_{12}K_{34}Q_1Q_4R_L}{K_{23}^*\sqrt{L_1L_4}\omega_0} \tag{4.6}$$

In this research, we propose to charge the EV from the roadside. Hence, EV is charged continuously when it runs into the charging area. The investigated

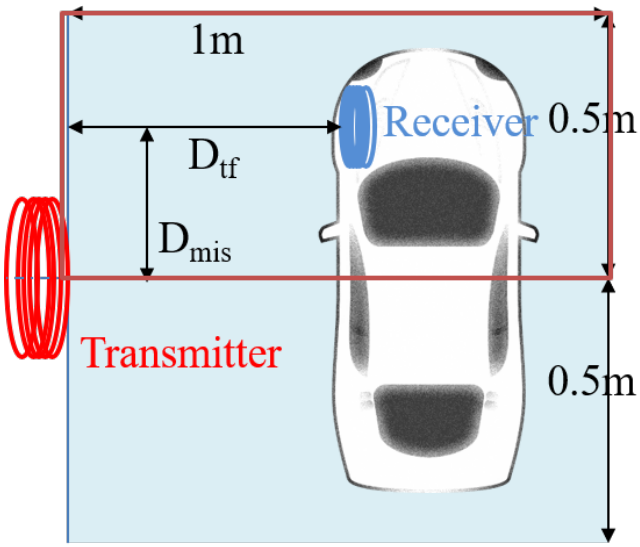


Figure 4.3: The charging area of the wireless dynamic charging

area is about 1 m distance and 0.5 m misalignment from the transmitter (Fig. 4.3).

The efficiency of coupling system is investigated in charging area. At operating frequency (13.56 MHz), the efficiency is high at an only constant transfer distance and misalignment condition (Fig. 4.4). The Fig. 4.4(a) is the efficiency of the coupling system at Dmis = 0. The highest efficiency is 91.2% at $D_{tf}$ = 55 cm. The Fig. 4.4(b) shows the efficiency at $D_{tf}$ = 5 cm. The maximum efficiency is 90.5% at 35 cm of misalignment. The distribution of efficiency in the charging area will be shown in the next section. Therefore, the average receiving power of EV is not high. The reason for this phenomenon is explained by equations (4.4) to (4.6).

### 4.1.2 The solution

At certain transfer position, the coupling coefficient $K_{23}$ is constant. The efficiency $\eta$ or $|S_{21}|$ is depends on the coupling coefficients $K_{12}$ and $K_{34}$. Because of the proposed system, it is difficult to transform the receiver parameters. Our proposed solution to improve the efficiency is changing the $K_{12}$. The maximum

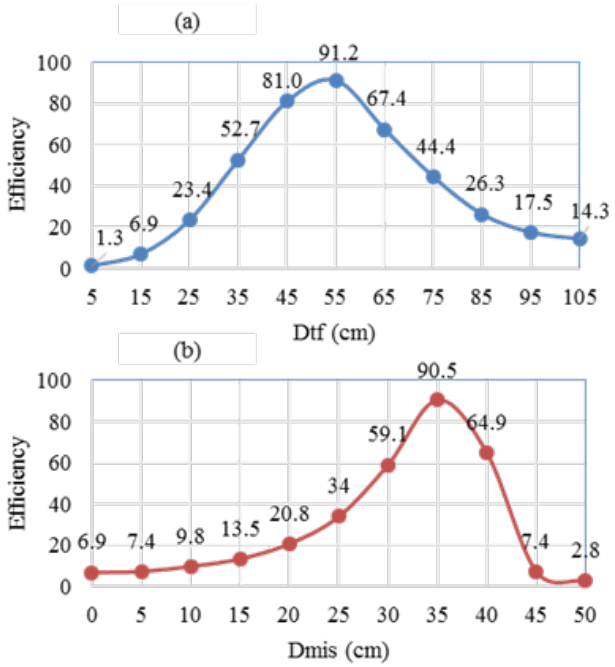


Figure 4.4: The efficiency verus the Dtf (a) and Dmis (b)

of $|S_{21}|$ is obtain when:

$$\frac{d|S_{21}|}{dK_{12}} = 0 \Leftrightarrow K_{12}^{*} = \sqrt{\frac{1 + K_{23}^{2}Q_2Q_3 + K_{34}^{2}Q_3Q_4}{Q_1Q_2 + K_{34}^{2}Q_1Q_2Q_3Q_4}} \tag{4.7}$$

Moreover, the coupling coefficient between coils is calulate as:

$$K_{ij} = \frac{M_{ij}}{\sqrt{L_jL_j}}; \quad i, j = 1 \sim 4 \tag{4.8}$$

An approximation of the mutual inductance given as equation (4.9) [15]:

$$M_{ij} = \pi\mu_0(r_ir_j)^2\frac{N_iN_j}{2D_{ij}^3} \tag{4.9}$$

$$K_{ij} \sim \frac{1}{D_{ij}^3} \tag{4.10}$$

With euqation (4.10) the variation of the $D_{12}$ and $D_{23}$ can be represented to the variation of $K_{12}$ and $K_{23}$. The variation of the mutual inductance or coupling coefficient ($K_{23}$) between transmitting side and receiving side when relative position is changed. The dependence of coupling coefficient on receiving position is shown in Fig. 4.5.

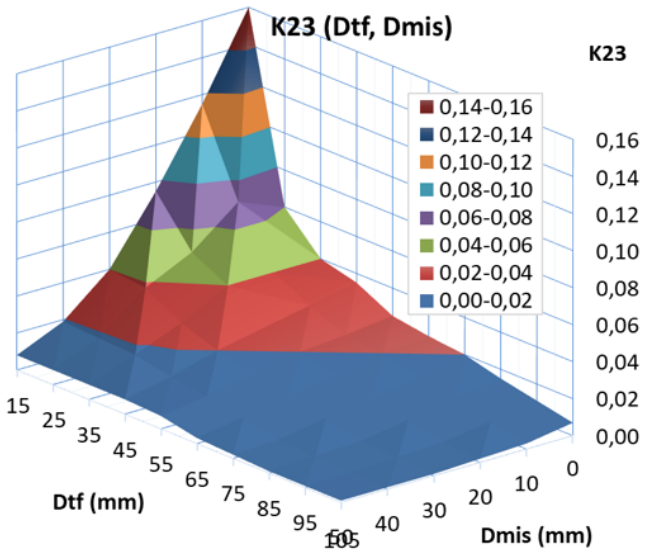


Figure 4.5: The dependence of K23 to the Dtf and Dmiss

The efficiency of coupling system can be calculated from the s-parameter and the parameters of the system. It does not only depend on the $K_{23}$ but also depend on $K_{12}$ and $K_{34}$ (the coupling coefficiencies in Fig. 3.9). Therefore, the efficiency can be improved by changing $K_{12}$ and $K_{34}$ when $K_{23}$ is changed. By the way, the $K_{12}$ and $K_{34}$ depend on the distance of the link coil and a resonant coil ($D_{12}$) (Fig. 4.1). In this system, the changing of $K_{34}$ is difficult because the receiver is in the EV (Fig. 4.3). So we propose changing the $D_{12}$ which is the distance between the link coil and the resonant coil of the transmitting side to improve the efficiency of the charging area.

## 4.2 The simulation

### 4.2.1 Electrical circuit simulation

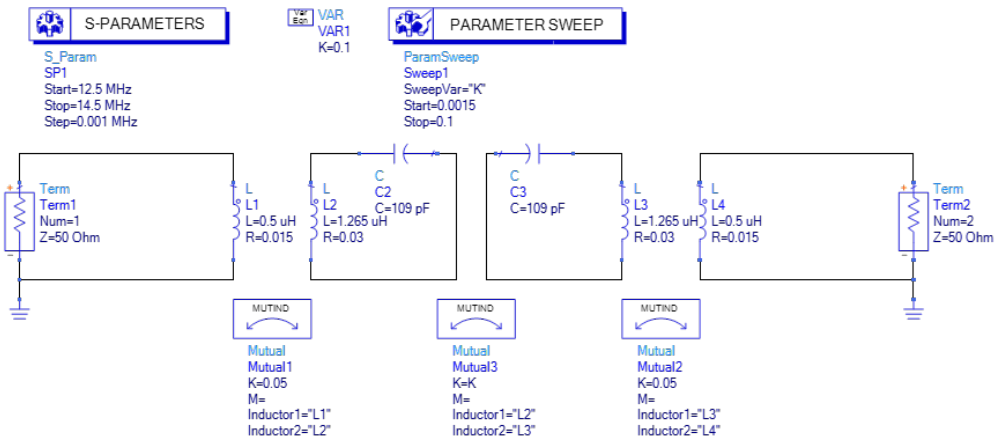


Figure 4.6: The simulation circuit

To verify the proposed solution, the coupling system will be simulated with equivalent circuit (Fig. 4.6). At first, the coupling coefficient $K_{12}$ and $K_{34}$ are set at 0.05 and the coupling coefficient $K_{23}$ is changed to confirm the resonant point and the direction of $K_{23}$ effect to resonant frequency and efficiency. When the $K_{23}$ is increased, the resonant frequency is split. Therefore, the efficiency at 13.56 MHz is reduced in both condition. As description in Fig. 4.7, the maximum resonant point at 13.56 MHz is the point which $K_{23} = 0.02$. With $K_{23} = 0.046$, the maximum efficiency is also high but the resonant frequency is split. In order to reach highest efficiency at 13.56 MHz, the $K_{12}$ and $K_{34}$ should be changed at the same time. The simulation result is shown in Fig 4.8. In addition, the result when only $K_{12}$ is changed is shown in Fig. 4.9. In both conditions, with the certain value of $K_{12}$ and $K_{34}$, the system has high efficiency at 13.56 MHz

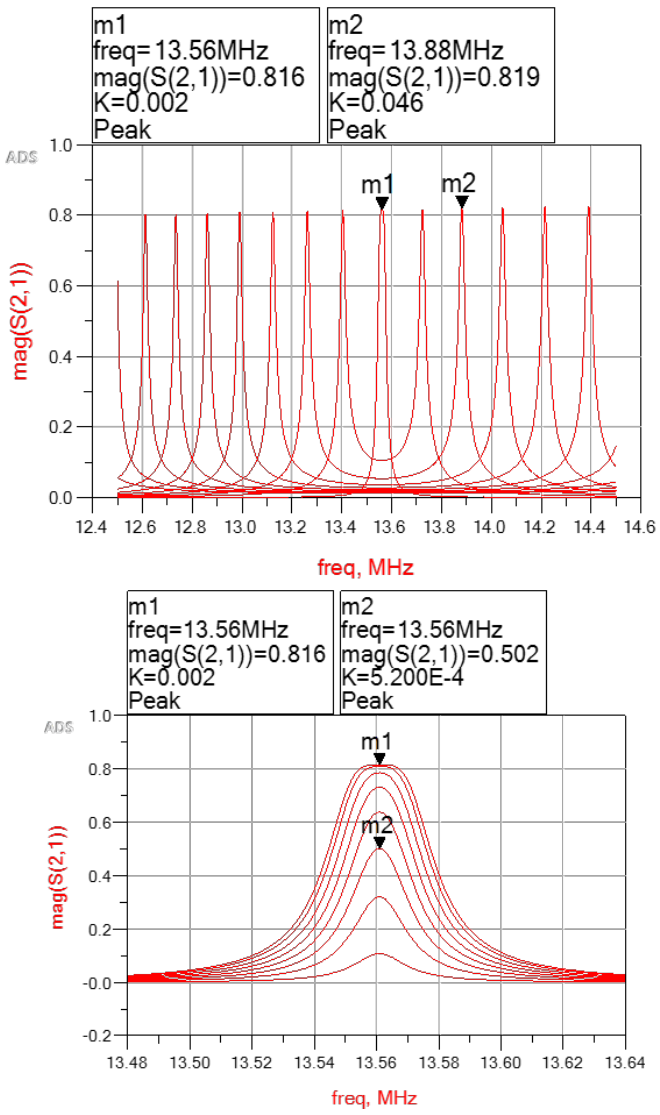


Figure 4.7: The simulation result when K23 is changed

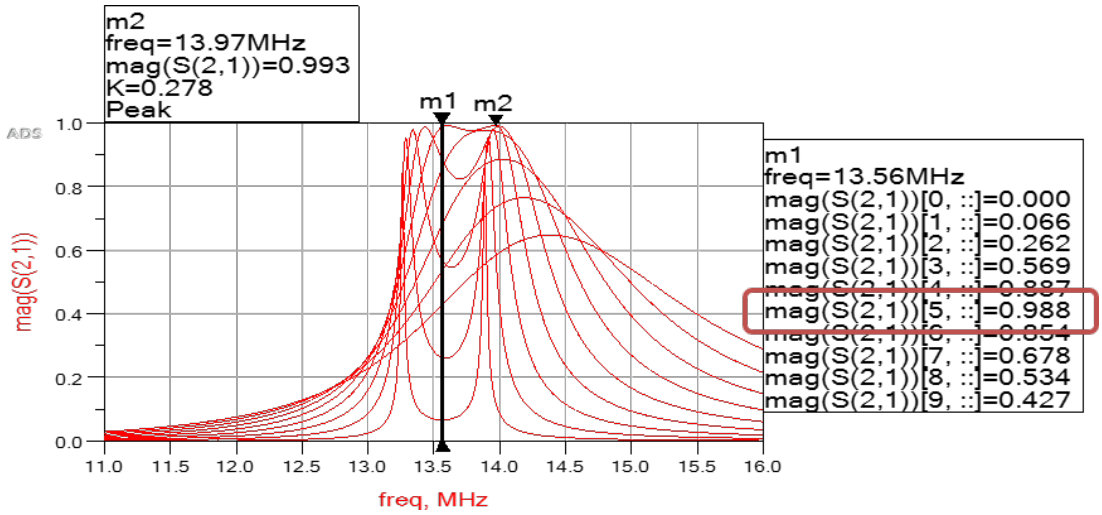


Figure 4.8: The simulation result when K23=0.046; K12=K34=[0.001,0.05]

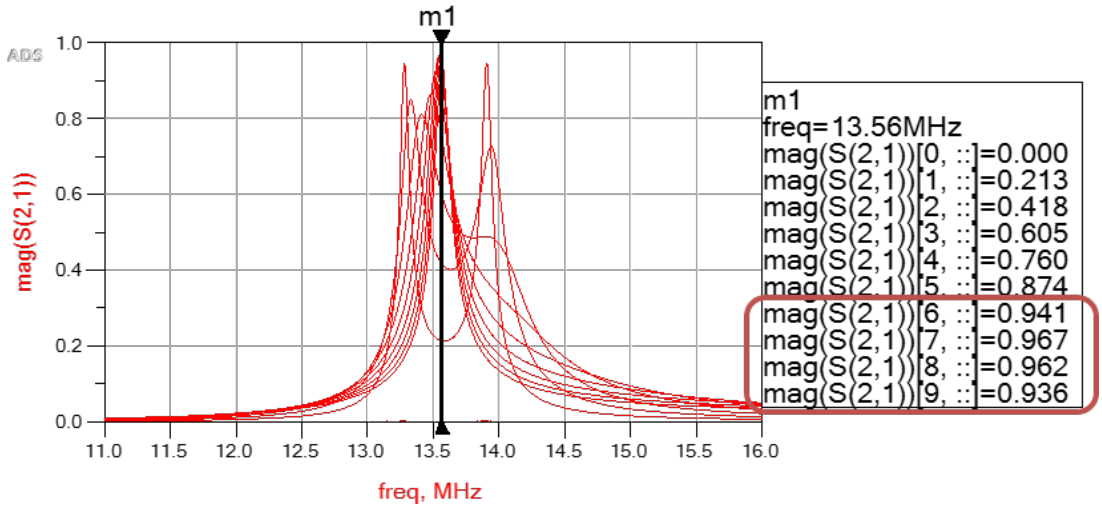


Figure 4.9: The simulation result when K23=0.046; K34=0.01; K12=[0.001,0.09]

### 4.2.2 Finite element simulation

The coupling system is simulated by FEA to verify the proposed solution. The simulating area is 15 cm to 105 cm of transfer distance and 0 cm to 50 cm misalignment. The transfer distance and misalignment are divided into each 10cm. The efficiency of coupling system is shown in Fig 4.10. It is presented in two conditions: without and with the proposed solution in Fig. 4.10(a) and Fig. 4.10(b) respectively. In the green area, the efficiency is higher than 80%. The blue area has 60% to 80% efficiency. The light blue area has the lowest efficiency (below 10%). Without improvement, the high-efficiency area is the middle area and it is small. The efficiency decreases when the transfer distance or misalignment differ to the middle area. With the proposed solution, the efficiency is increased in the red line border area which has 65 cm and 40 cm of Dtf and Dmis respectively. In others area, the performance cannot be improved. At last, the average charging efficiency is increased. The Fig. 4.11 shows more detail about the improved efficiency at Dmis=0 cm. The maximum increased efficiency is 56.4%. The $D_{12}$ is changed due to the proposed solution. The variation of $D_{12}$ is shown in Fig. 4.12.

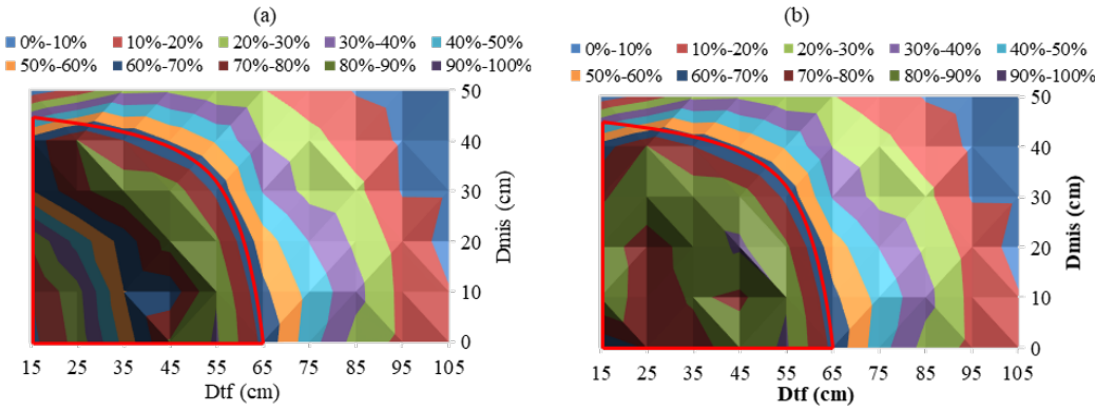


Figure 4.10: The efficiency of antenna in charging area in simulation; (a) The efficiency without improvement; (b) The efficiency with the improvement

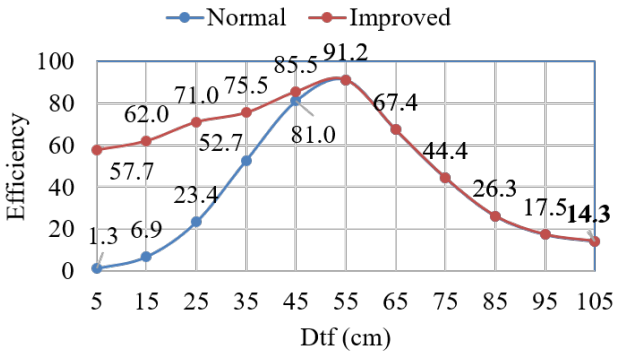


Figure 4.11: The comparision of the antenna efficiency in simulation with $D_{miss} = 0cm$

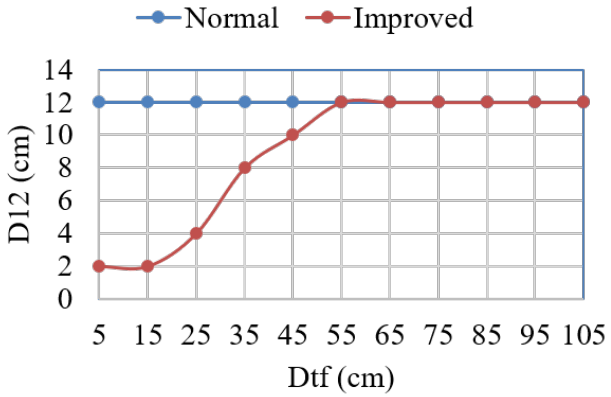


Figure 4.12: The variation of $D_{12}$ to improve the antenna efficiency in simulation

## 4.3 The experiment

The experimental system is shown in Fig. 4.13 and Fig. 4.14. The position of the receiver is input to the microcomputer. Depend on the lookup data of $D_{12}$ to obtain the highest efficiency, the matching system adjusts the position of the powered coil in the transmitter. The results of the experiment are shown in Fig. 4.15, Fig. 4.16 and Fig. 4.17. In comparison with the simulation results, the distribution of charging efficiency is similar.

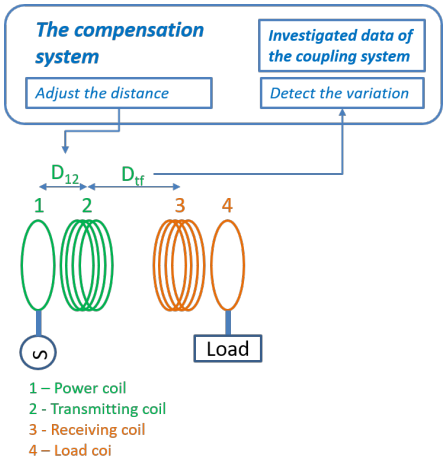


Figure 4.13: The diagram of the experimental system

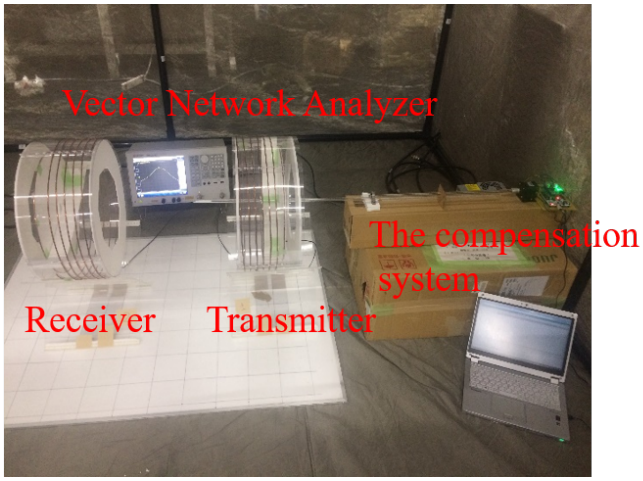


Figure 4.14: The experimental system

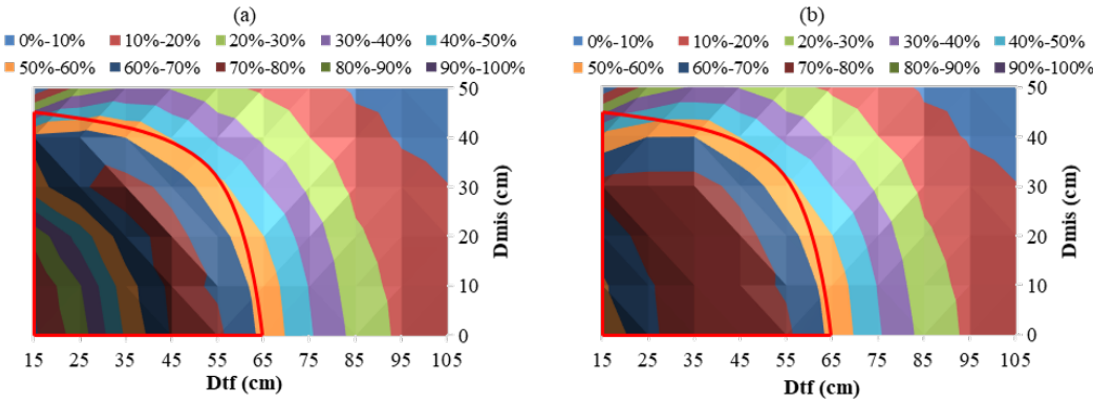


Figure 4.15: The efficiency of antenna in charging area in experiment; (a) The efficiency without improvement; (b) The efficiency with the improvement

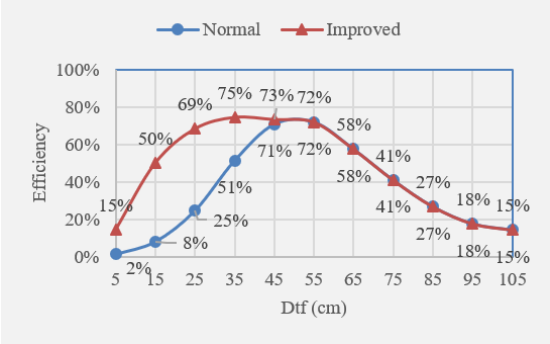


Figure 4.16: The comparision of the antenna efficiency in experiment with Dmiss=0cm

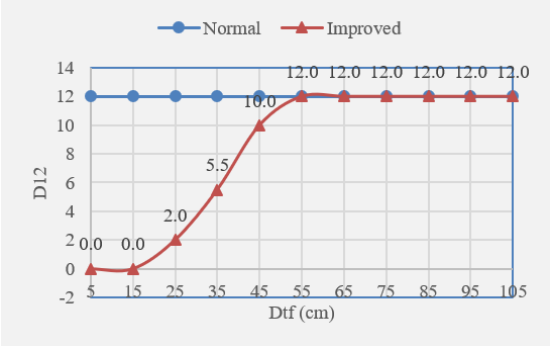


Figure 4.17: The variation of $D_{12}$ to improve the antenna efficiency in experiment

# Chapter 5

# Conclusion And Future Work

## 5.1 Conclusion

This thesis presented the 13.56 MHz antenna design for wireless power transfer system with over 90% efficiency in simulation. And the efficiency of the antenna is improvement in charging area of the dynamic wireless charging. The summary of the thesis research works as following:

• The difficulty of the 13.56 MHz antenna design is obtaining the high efficiency and narrow band of high operating frequency. The analysis shows that it's difficult to design the high frequency with the calculation because of the parasitic elements. The more simple method is the two ports network analysis. The scattering parameter can be used to estimate the efficiency of the antenna. The finite element analysis and the vector network analyzer can export the s-parameter of the antenna simulation and experiment. Therefore the antenna's efficiency is calculated.

• In the dynamic wireless charging, the position of the receiver is variant. Moreover, the operating frequency of the antenna is narrow (ISM band) and the antenna's efficiency is sensitive with the receiver position variation. Therefore, the compensation system is required in efficiency improvement. The designed system improved the efficiency of the antenna in the certain area.

## 5.2 Future Work

The high efficiency 13.56 MHz antenna is designed. However, the high power is not transfered. The lossless of the antenna is not analyzed. Therefore, the future research is design the high power antenna at 13.56 MHz to apply in EV charging system. The transfer distance is also increased.

The designed compensate system can improve the efficiency of the antenna but it can's work with the high speed movement of the receiver. Therefore, the improvement of the system will be design.

# References


[1] A. N. Azad, A. Echols, V. A. Kulyukin, R. Zane, and Z. Pantic. Analysis, optimization, and demonstration of a vehicular detection system intended for dynamic wireless charging applications. *IEEE Transactions on Transportation Electrification*, **5**(1):147–161, March 2019.

[2] J. G. Bolger, F. A. Kirsten, and L. S. Ng. Inductive power coupling for an electric highway system. In *28th IEEE Vehicular Technology Conference*, **28**, pages 137–144, March 1978.

[3] W. C. Brown. The history of power transmission by radio waves. *IEEE Transactions on Microwave Theory and Techniques*, **32**(9):1230–1242, Sep. 1984.

[4] H. Choi, S. Lee, and C. Cha. Optimization of geometric parameters for circular loop antenna in magnetic coupled wireless power transfer. In *2014 IEEE Wireless Power Transfer Conference*, pages 280–283, May 2014.

[5] G. A. Covic and J. T. Boys. Modern trends in inductive power transfer for transportation applications. *IEEE Journal of Emerging and Selected Topics in Power Electronics*, **1**(1):28–41, March 2013.

[6] S. Cui, B. Song, X. Gao, and S. Dong. A narrow-width three phase magnetic coupling mechanism with constant output power for electric vehicles dynamic wireless charging. In *2018 IEEE PELS Workshop on Emerging Technologies: Wireless Power Transfer (Wow)*, pages 1–6, June 2018.

[7] X. Dai, J. Jiang, Y. Sun, Y. Su, C. Tang, and Z. Wang. Misalignment tolerance analysis of dynamic wireless charging system based on dual excitation units. In *2018 IEEE PELS Workshop on Emerging Technologies: Wireless Power Transfer (Wow)*, pages 1–5, June 2018.

[8] X. Dai, J. Jiang, and J. Wu. Charging area determining and power enhancement method for multiexcitation unit configuration of wirelessly dynamic charging ev system. *IEEE Transactions on Industrial Electronics*, **66**(5):4086–4096, May 2019.

[9] G. Grandi, M. K. Kazimierczuk, A. Massarini, and U. Reggiani. Stray capacitances of single-layer solenoid air-core inductors. *IEEE Transactions on Industry Applications*, **35**(5):1162–1168, Sep. 1999.

[10] R. E. Hamam, A. Karalis, J. D. Joannopoulos, and M. Soljiacic. Coupled-mode theory for general free-space resonant scattering of waves. In *Physiacl review A*, **Vol 75**, pages issue5, ID 053801, 2007.

[11] SAE J2954. In *http://standards.sae.org/wip/j2954*.

[12] S. Jeong, Y. J. Jang, and D. Kum. Economic analysis of the dynamic charging electric vehicle. *IEEE Transactions on Power Electronics*, **30**(11):6368–6377, Nov 2015.

[13] S. Jeong, Y. J. Jang, D. Kum, and M. S. Lee. Charging automation for electric vehicles: Is a smaller battery good for the wireless charging electric vehicles? *IEEE Transactions on Automation Science and Engineering*, **16**(1):486–497, Jan 2019.

[14] S. Y. Jeong, J. H. Park, G. P. Hong, and C. T. Rim. Automatic current control by self-inductance variation for dynamic wireless ev charging. In *2018 IEEE PELS Workshop on Emerging Technologies: Wireless Power Transfer (Wow)*, pages 1–5, June 2018.

[15] A. Karalis, J.D. Joannopoulos, and M. Soljacic. Efficienct wireless non-radiative mid-range energy transfer. In *Elsevier Annals of Physics*, **323**, pages 34–48, 2008.

[16] D. W. Knight. In *http://www.g3ynh.info/zdocs/magnetics*.

[17] A. K. A. Kurs, R. Moffatt, J.D. Joannopoulos, P. Fisher, and M. Soljacic. Wireless power transfer via strongly coupled magnetic resonances. In *Science*, **317**, pages 83–86 Vol.317 No.5834, 2007.

[18] S. Li and C. C. Mi. Wireless power transfer for electric vehicle applications. *IEEE Journal of Emerging and Selected Topics in Power Electronics*, **3**(1):4–17, March 2015.

[19] B. Liu, Z. Chen, and H. Hsu. Implementation of high efficiency coupling coil in wireless power transfer system. In *2018 IEEE Wireless Power Transfer Conference (WPTC)*, pages 1–4, June 2018.

[20] C. Liu, C. Jiang, and C. Qiu. Overview of coil designs for wireless charging of electric vehicle. In *2017 IEEE PELS Workshop on Emerging Technologies: Wireless Power Transfer (WoW)*, pages 1–6, May 2017.

[21] H. Mansor, M. Halim, M. Mashor, and M. Rahim. Application on wireless power transmission for biomedical implantable organ. In *Springer-Verlag Biomed*, **21**, pages 40–43, 2008.

[22] R. Matias, B. Cunha, and R. Martins. Modeling inductive coupling for wireless power transfer to integrated circuits. In *2013 IEEE Wireless Power Transfer (WPT)*, pages 198–201, May 2013.

[23] E. Maulana, Z. Abidin, and W. Djuriatno. Wireless power transfer characterization based on inductive coupling method. In *2018 Electrical Power, Electronics, Communications, Controls and Informatics Seminar (EECCIS)*, pages 164–168, Oct 2018.

[24] R. Mecke and C. Rathge. High frequency resonant inverter for contactless energy transmission over large air gap. In *2004 IEEE 35th Annual Power Electronics Specialists Conference (IEEE Cat. No.04CH37551)*, **3**, pages 1737–1743 Vol.3, June 2004.

[25] R. G. Medhurst. H.f resistance and self-capacitance of single layer solenoids. *Wireless Eng*, **Vol. 24**:pp35–43, February 1947.

[26] B. Minnaert and N. Stevens. Maximizing the power transfer for a mixed inductive and capacitive wireless power transfer system. In *2018 IEEE Wireless Power Transfer Conference (WPTC)*, pages 1–4, June 2018.

[27] A. J. Moradewicz and M. P. Kazmierkowski. Contactless energy transfer system with fpga-controlled resonant converter. *IEEE Transactions on Industrial Electronics*, **57**(9):3181–3190, Sep. 2010.

[28] H. Nagaoka. The inductance coefficient of solenoids. In *Journal of the College of Science, Imperial University*, **vol. XXVII**, pages article 6, Tokyo, 1909.

[29] P. Ning, J. M. Miller, O. C. Onar, and C. P. White. A compact wireless charging system for electric vehicles. In *2013 IEEE Energy Conversion Congress and Exposition*, pages 3629–3634, Sep. 2013.

[30] S. J. Orfanidis. Electromagnetic waves and antennas. In *ECE Department Rutgers University, NJ*, pages 8054–8058, Sep. 2008.

[31] E. B. Rosa. Scientific papers. In *Formulas and Tables for the Calculation of Mutual and Self-Inductance*, pages 1 p., 237 p., 1916.

[32] A. P. Sample, D. T. Meyer, and J. R. Smith. Analysis, experimental results, and range adaptation of magnetically coupled resonators for wireless power transfer. *IEEE Transactions on Industrial Electronics*, **58**(2):544–554, 2011.

[33] Seokhwan Lee, Guho Jung, Seungyong Shin, Yangsu Kim, Boyune Song, Jaegue Shin, and D. Cho. The optimal design of high-powered power supply modules for wireless power transferred train. In *2012 Electrical Systems for Aircraft, Railway and Ship Propulsion*, pages 1–4, Oct 2012.

[34] R. Shadid and S. Noghanian. Hybrid power transfer and wireless antenna system design for biomedical implanted devices. In *2018 International Applied Computational Electromagnetics Society Symposium (ACES)*, pages 1–2, March 2018.

[35] N. Shinohara. Wireless power transmission progress for electric vehicle in japan. In *2013 IEEE Radio and Wireless Symposium*, pages 109–111, Jan 2013.

[36] K. Song, C. Zhu, Kim Ean Koh, T. Imura, and Y. Hori. Wireless power transfer for running ev powering using multi-parallel segmented rails. In *2015 IEEE PELS Workshop on Emerging Technologies: Wireless Power (2015 WoW)*, pages 1–6, June 2015.

[37] S. Song, Q. Zhang, C. Zhu, and D. Wang. A practical static simulator for dynamic wireless charging of electric vehicle using receiver open circuit voltage equivalent. In *2017 IEEE Energy Conversion Congress and Exposition (ECCE)*, pages 4859–4864, Oct 2017.

[38] T. Stamati and P. Bauer. On-road charging of electric vehicles. In *2013 IEEE Transportation Electrification Conference and Expo (ITEC)*, pages 1–8, June 2013.

[39] V. F. Tseng and H. Xie. Resonant inductive coupling-based piston position sensing mechanism for large vertical displacement micromirrors. *Journal of Microelectromechanical Systems*, **25**(1):207–216, Feb 2016.

[40] S. Wang, D. G. Dorrell, Y. Guo, and M. Hsieh. Inductive charging coupler with assistive coils. *IEEE Transactions on Magnetics*, **52**(7):1–4, July 2016.

[41] Y. Wang, J. Song, L. Lin, X. Wu, and W. Zhang. Research on magnetic coupling resonance wireless power transfer system with variable coil structure. In *2017 IEEE PELS Workshop on Emerging Technologies: Wireless Power Transfer (WoW)*, pages 1–6, May 2017.

[42] H. H. Wu, A. Gilchrist, K. D. Sealy, and D. Bronson. A high efficiency 5 kw inductive charger for evs using dual side control. *IEEE Transactions on Industrial Informatics*, **8**(3):585–595, Aug 2012.

[43] W. Xiong, M. Jiang, G. Huang, and H. Chen. Analysis on transfer efficiency of five different antenna configurations in short-distance wireless power transfer. In *2018 IEEE International Conference on Electron Devices and Solid State Circuits (EDSSC)*, pages 1–2, June 2018.

[44] A. A. Zaky and R. Hawley. Fundamentals of electromagnetic field theory. *Harrap*, September 1974.

[45] Z. Zhang, H. Pang, C. H. T. Lee, X. Xu, X. Wei, and J. Wang. Comparative analysis and optimization of dynamic charging coils for roadway-powered electric vehicles. *IEEE Transactions on Magnetics*, **53**(11):1–6, Nov 2017.

# Research Achievements

### Transaction

[I.1] N. T. Cuong, N. K. Trung and K. Akatsu, "A 13.56 MHz Antenna Design With The Efficiency Improvement For The Wireless Power Transfer System." IEEJ Journal of Industry Applications (English only), 2020, Submitted.

### International Conference Paper

[I.1] N. T. Cuong and K. Akatsu, "Efficiency improvement for multi-position of receiving side in wireless power transfer coupling system at 13 . 56 MHz." EVS31-EVTECH, Kobe, 2018.

[I.2] N. T. Cuong and K. Akatsu,"Efficiency Improvement For Multi-Position of Receiver in 13 . 56 MHz Wireless Power Transfer Coupling System." in PEAC'2018, Shenzhen, China, pp. 3–7, 2018.

### Domestic Conference Paper

[D.1] N. T. Cuong and K. Akatsu, "Efficiency improvement for multi-position of receiving side in wireless power transfer coupling system at 13 . 56 MHz." JIASC, Hakodate, pp. 205–208, 2017.

### Other Paper

## RESEARCH ACHIEVEMENTS

[O.1] N. T. Cuong and K. Akatsu, "Basic Experiment on 13.56 MHz Coupling System of Wireless Power Transfer For Electric Vehicle Dynamic Charging." SEATUC, Tokyo, p. 4, 2016.

[O.2] N. T. Cuong and K. Akatsu, "Efficiency Analysis of Distance Variations in WPT Coupling System at 13 . 56 MHz." S2PC, Nagaoka, pp. 4–5, 2016.